REVIEW ARTICLE

Charge-coupled device area x-ray detectors

Sol M. Gruner[a)]
Department of Physics, Laboratory of Atomic and Solid State Physics, Cornell University, Ithaca, New York 14853 and Cornell High Energy Synchrotron Source (CHESS), Cornell University, Ithaca, New York 14853

Mark W. Tate
Department of Physics, Laboratory of Atomic and Solid State Physics, Cornell University, Ithaca, New York 14853

Eric F. Eikenberry
SLS-Project, Paul Scherrer Institut, CH-5232 Villigen PSI, Switzerland

(Received 3 January 2002; accepted for publication 21 April 2002)

Charge-coupled device (CCD) area x-ray detector technology is reviewed. CCD detectors consist of a serial chain of signal components, such as phosphors, fiber optics or lenses, image intensifiers and the CCD which serve to convert the x-ray energy to light or electron-hole pairs and to record the spatially resolved image. The various combinations of components that have been used to make CCD detectors are described and the properties of each of the critical components are discussed. Calibration and correction procedures required for accurate data collection are described. The review closes with a brief description of future directions for solid-state area x-ray detectors. © *2002 American Institute of Physics.* [DOI: 10.1063/1.1488674]

I. INTRODUCTION

Charge-coupled device (CCD)-based area x-ray detectors (hereafter simply called simply ''CCD detectors'') have enormously improved the quality and speed of x-ray data acquisition for many scattering and imaging applications. CCD detectors are the outgrowth of several decades of development of area x-ray detectors based on electro-optical imagers (e.g., vidicons, CCDs, and diode arrays) and share the general characteristics of modularity, being composed of a sequential cascade of components that were usually developed for other applications. On the one hand, this modularity provides the detector designer with a wealth of choices; on the other hand it provides a bewildering number of possibilities. The primary purpose of this article is to review the considerations involved in optimizing a detector for a given application, and thereby serve as a guide to the detector designer or user.

A secondary goal of this review is to provide a context for related x-ray detector developments. Much of the technology of CCD-based detectors, such as procedures for area detector calibration, turn out to also be useful for other types of x-ray detectors. CCD detectors also provide the basis for the next generation of pixel array detectors (PADs) now under development in laboratories across the world. Thus, a good understanding of CCD-detector principles is also useful in a wider context. This review complements many excellent papers on CCD detectors already in the literature. For some general references, see Refs. 1–7.

II. ELECTRO-OPTICAL AREA X-RAY DETECTOR COMPONENTS

A. Overview

CCD detectors most generally consist of a relay of electro-optical elements (Fig. 1) that function to stop the x rays and generate a primary signal that is, perhaps, amplified and eventually coupled to a CCD. CCD detectors are distinguished one from the other by the components that perform these functions. An understanding of the signal relay requires an analysis of the five functions performed by the signal relay components:

(1) *X-ray conversion* involves stopping the x ray in, for example, a phosphor or semiconductor layer and the conversion of the x-ray energy into more readily manipulated visible light or electron quanta.
(2) *Intensification* of the resultant signal may be required if the signal is weak.
(3) Various *coupling methods* (e.g., lenses, fiber optics) are used to couple the signal relay components.
(4) An *imaging array*, e.g., the CCD, position encodes the resultant signal.
(5) The *operating mode* of the imaging array (e.g., whether it is read out at video rates or in a cooled, slow-scan, low-noise rate) strongly determines the selection of the components and the signal-to-noise ratio of the detector.

[a)]Author to whom correspondence should be addressed; electronic mail: smg26@cornell.edu

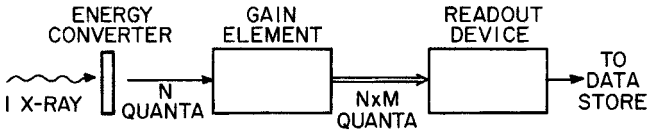

FIG. 1. Electro-optical x-ray detectors consist of a relay of signal elements. The energy converter stops the x ray and produces N visible light photons or electrical charges. These are amplified by a gain element, such an image intensifier, to produce $N \times M$ quanta that are relayed to a readout device, such as a CCD.

The design of the signal relay is dictated by the x-ray application and the practical constraints of available components. As examples, CCDs are directly sensitive to x rays and make excellent soft x-ray detectors without additional components.[7] However, the available CCDs may be too small, too susceptible to radiation damage, or have too low an x-ray stopping power for a given application. An alternative is to absorb the x rays in a larger area, radiation-hard, higher stopping power phosphor screen and couple the resultant light onto a CCD. The drawback here is that while an x-ray stopped in a CCD may create thousands of signal electrons, only a few tens of electrons may result from a relatively inefficient combination of a phosphor-CCD optical relay, thereby necessitating the imposition of a light amplifier between the phosphor and the CCD. Thus, it is necessary to understand the properties and efficiencies of the various components in the optical relay in order to winnow down the number of possible configurations.

Figure 2 shows examples of CCD detector systems to help set the context for the discussion that follows.

B. X-ray converters

The function of the x-ray converter is to stop the x rays and produce more readily manipulated quanta, such as visible photons or electrons. We discuss phosphors and semiconductors, which are by far the most important converters in current use.

1. Phosphors

The use of x-ray phosphors dates back to the first discovery of x rays when, in 1895, Roentgen noticed the glow of a barium platino-cyanide screen next to his discharge tube. Although Roentgen soon turned to photographic emulsions to permanently record his findings, it was quickly realized that photographic emulsions had very low x-ray stopping power and that sensitivity could be gained by pressing a thin, higher stopping power phosphor sheet against the emulsion. Pupin had already proposed $CaWO_4$ for this purpose in 1896.[8]

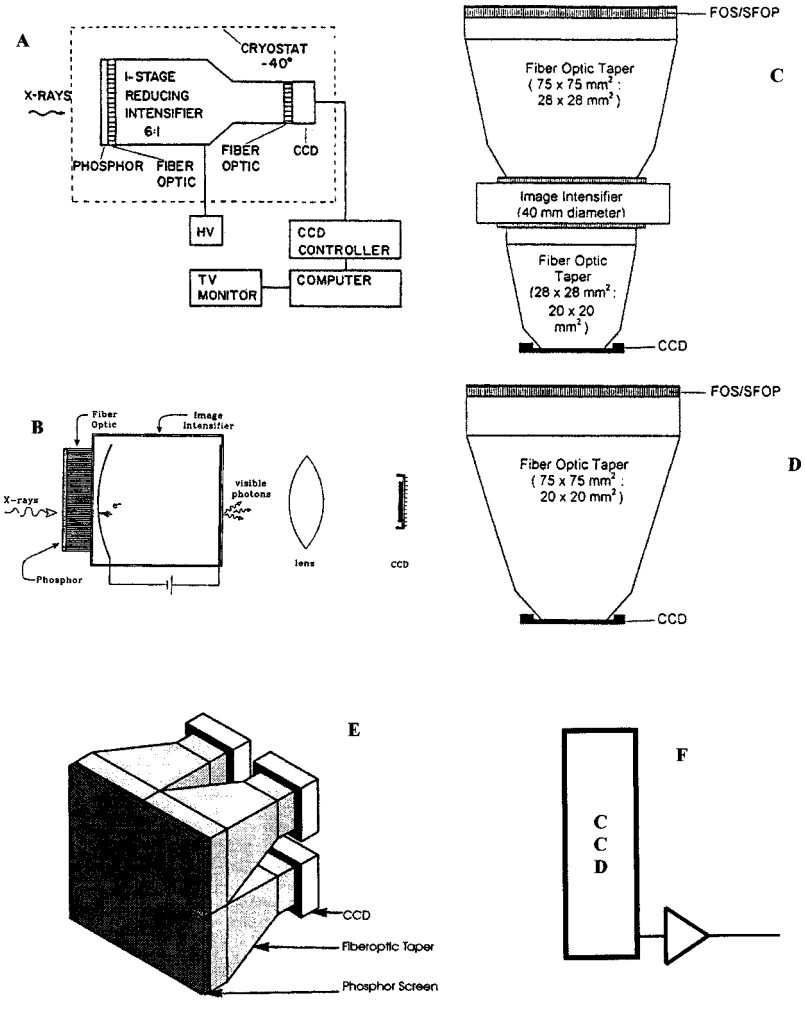

FIG. 2. CCD detector configurations consist of various combinations of luminescent screens, fiber-optic plates and tapers, lenses, image intensifiers, and CCDs. Some examples: (A) Phosphor screen fiber-optically coupled to a reducing image intensifier, that is fiber-optically coupled to a CCD (Ref. 150); (B) phosphor screen fiber-optically coupled to an image intensifier that is lens coupled to a CCD (Ref. 1); (C) phosphor or scintillating fiber-optics screen coupled to a fiber-optic taper, image intensifier, a second taper, and the CCD (Ref. 87); (D) phosphor or scintillating fiber-optics screen coupled to a fiber-optic taper and the CCD (Ref. 87); (E) a matrix of closely fitting phosphor screen-taper-CCD modules (Ref. 2); and (F) direct conversion of x rays into electrical signals within the CCD.

TABLE I. Some characteristics of phosphors commonly used for analytical x-ray CCD detectors. The initial decay is fast if it is less than a millisecond, slow if it is greater than 1 millisecond. The persistence is very high if it is very visible to the eye.

	CsI:Tl	NaI:Tb	ZnS:Ag	Gd_2O_2S:Tb	(Zn,Cd)Se
Robustness	hydroscopic	very hydroscopic	stable	stable	
Efficiency (%)	10	13	20	15	19
Initial light decay	fast	slow	fast	slow	fast
Persistence	low	low	very high	low	low
Color	green	green	blue	green	red

Not surprisingly, a very large number of phosphors have been developed in the century since Roentgen's discovery. Phosphors have very complex chemistry and physics and are used for a diverse variety of applications, ranging from medical and analytical x-ray detection to fluorescent lighting, cathode ray tubes and television projection systems, resulting in a literature that is large and spread out over many years and in many journals. An unfortunate consequence of the economic importance of phosphor-based devices is that much industrial phosphor research has been proprietary and is not in the open literature. Industrial work on phosphors was especially intense during the twenty years following World War II due to the rapidly evolving needs of the television and lighting industries. Tragically, much of the unpublished phosphor expertise developed during that time is now being lost as old company records are discarded and the original researchers pass away. Even though the use of phosphors is larger than ever, there is relatively little new phosphor research being performed today. Hopefully this situation will change with the advent of combinatorial approaches[9,10] and new sol-gel processes.[11]

A superb review of modern phosphors, with chapters devoted to x-ray applications, is Blasse and Grabmaier.[12] Garlick,[13] Leverenz,[14] and Curie[15] are classic books on phosphor physics. Birks[16] covers scintillators. Other reviews include Ouweltjes,[17] D'Silva and Fassel,[18] and Blasse.[19–21] TEPAC[22] is an invaluable reference for cathode ray tube phosphors. Phosphor characteristics and valuable advice are also listed in the information available from phosphor manufacturers (see, e.g., Refs. 23–26).

Our concern in this section is with solid-state materials which luminesce (emit light) when irradiated by x rays—we shall generally call all such materials phosphors. We prefer to call materials ''luminescent,'' rather than ''fluorescent'' or ''phosphorescent'' because the distinction between fluorescence as a spin-allowed transition ($\Delta S=0$) and phosphorescence as a spin-forbidden transition ($\Delta S=1$) is not universally applied (e.g., for discussion see Ref. 27; Appendix 3 of Blasse and Grabmaier[12]). Similarly, there are no universally used definitions which distinguish scintillator and phosphor materials. We will follow the common practice of calling materials scintillators if they are usually used in photon counting applications and phosphors if they are usually used in photon integrating applications. The reader should be aware, however, that the term ''scintillators'' and ''phosphors'' often refer to the same materials. To be unambiguous, they are both luminescent materials.

A phosphor screen is a thin layer of phosphor that is used to convert an x-ray image into a light image. Phosphor screen characteristics of importance for CCD detector x-ray imaging include:

(i) robustness and stability;

(ii) x-ray stopping power;

(iii) spectral matching of the light output to the next optical relay element;

(iv) energy efficiency for conversion of x rays to light;

(v) luminescent decay time and afterglow;

(vi) linearity of light output with incident x-ray dose and intensity;

(vii) noise; and

(viii) spatial resolution across the screen.

Some important x-ray luminescent screen materials commonly used for analytical x-ray CCD detectors are listed in Table I and in Fig. 3. The selection of an x-ray phosphor for a given application invariably involves compromises among varied, and often conflicting characteristics of available phosphor materials. For example, the use of thin screens to optimize the spatial resolution compromises the x-ray stopping power. As another example, NaI:Tl, which is very energy efficient, is made of low-Z atoms and has a relatively low stopping power per unit thickness. Its spectral emission is also not well matched to the red sensitivity of many CCDs. The effective use of a phosphor requires knowledge of all its relevant characteristics and the ways in which these characteristics affect the use of the phosphor and its coupling to other detector components.

Relatively little recent research has focused on developing new x-ray phosphors,[20,28,29] mostly because phosphor development is difficult and potential markets are small (see, however, Refs. 30–35). A promising new ceramic phosphor is Gd_2O_2S:Pr,Ce,F.[9,10,33,36]

In order to be useful for two-dimensional imaging, the phosphor must be fashioned into a thin screen. Phosphor screens may consist of a single crystal,[37] or may be a thin polycrystalline sheet which is formed by vacuum evaporation or sublimation[38–42] or solution deposition.[42] Most commonly, however, screens consist of carefully milled powders that are settled, pressed, or otherwise deposited onto a substrate in the presence of a low concentration of a binding material.[43–49] An important reason to use powder screens is that many of the important x-ray phosphors are only available as fine powders.

1. Robustness and stability. Robustness and stability refer both to chemical and crystal structure changes that may affect the luminosity of the screen and to bulk physical changes, such as resistance to cracking or peeling. The ma-

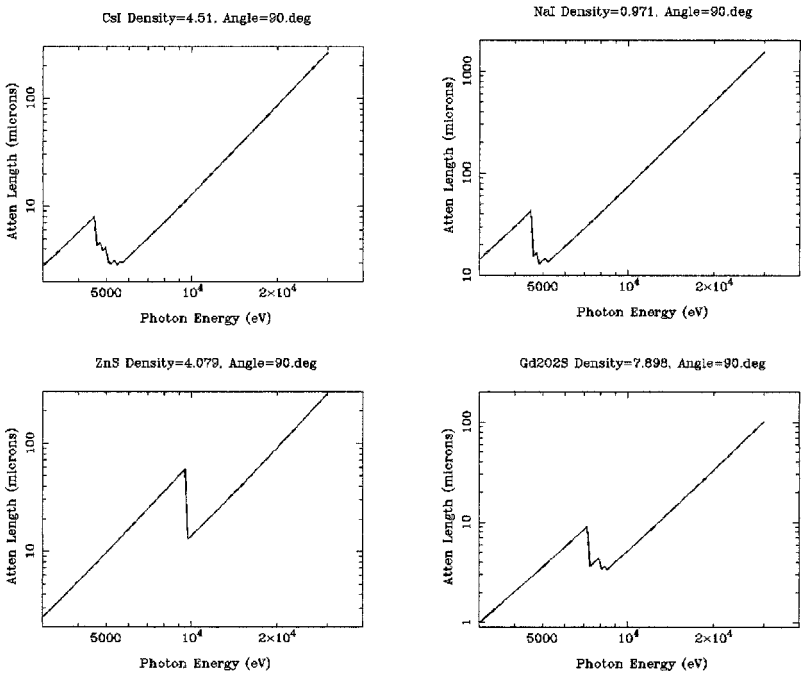

FIG. 3. The attenuation length is defined as the thickness of a material required to reduce the transmitted x-ray intensity to $1/e$ of its incident value. Attenuation lengths are shown for four of the phosphors of Table I. These figures were produced with the online calculator at http://www-cxro.lbl.gov/optical_constants/atten2.html.

terials listed in Table I are mostly radiation-hard solid-state materials, such as doped salts (e.g., CsI:Tl) or ceramics (e.g., Gd_2O_2S:Tb). Organic plastic scintillators[16] are available and easily made into thin screens, but they are rarely used in x-ray imaging applications because they have low x-ray stopping power and low energy efficiency ($\sim$3% or less). Although inorganic phosphors tend to be intrinsically radiation hard, modern synchrotron sources are capable of delivering x-ray doses that cause even glasses to rapidly develop color centers, and quickly degrade plastic binders and phosphor window materials.

CsI and NaI are very energy efficient phosphors. Both are hydroscopic and readily poisoned by water, which necessitates hermetic sealing behind water-vapor tight windows. It is desirable to make the windows as x-ray transparent as possible. Beryllium is totally impervious to water vapor and works well, but is expensive and highly toxic. Unfortunately, beryllium corrodes readily when exposed to liquid water, and, therefore, must be kept completely dry. Since many detectors involve cooled parts and suffer from water condensation on the window, it may be necessary to use heaters around the edge of the window to keep the beryllium above room temperature, a flow of dry gas across the window, or polymer or thin inorganic films to protect the beryllium. For low energy x rays, attention must also be given to beryllium purity. Heavy metals, such as iron, are common contaminants in beryllium at concentrations that substantially decrease the transparency for low energy x rays. Another problem with contaminants is that they introduce unexpected absorption edges that complicate the window transparency in polychromatic x-ray applications.

Aluminum foil windows are excellent light and water-vapor barriers, as long as the aluminum is pinhole free. Although aluminum is less x-ray transparent than beryllium, it is more readily available in very thin sheets. Since thin aluminum windows are delicate and easily ruptured, polymer/metal composite films are an attractive window alternative. Thin polymer films always have some permeability to air and water, and do not, in general, provide the long term protection against water entry afforded by metals; furthermore, they are rarely light tight. The food packaging industry also faces this problem because water, light, and oxygen degrade the quality and shelf-life of many packaged goods. In response, the food industry has developed a variety of thin polymer/aluminum film composites which work very well as long-term vapor and light barriers (e.g., a manufacturer of appropriate composite films is Fres-co System, Inc.[50]). Many of these packaging materials are also reasonably x-ray transparent and make excellent windows.

The x-ray window is ideally placed as close as possible to the phosphor to avoid difficulties of x-ray scatter from the window material. If the experiment requires a gap between the window and the phosphor, then careful consideration must be given to both the small angle and wide angle scatter from the window,[51] especially if the window precedes a beam stop for the primary x-ray beam.

2. X-ray stopping power. The minimum useful thickness of a luminescent screen is largely a compromise between its x-ray stopping power and it's spatial resolution. In general, thin screens are desirable in order to improve the spatial resolution across the screen, especially in cases in which the incident x rays strike the screen at a substantial angle to the screen normal. Phosphor screens are typically specified in terms of the areal density in mg/cm^2, which, for a given atomic composition allows direct computation of the x-ray stopping power at a given x-ray wavelength. The thickness of the screen is given by the areal density divided by the mass density. Since many screens are made of settled grains of phosphor powder, the mass density may be considerably less than the phosphor bulk crystal density. A typical settled screen is about 50% void volume. Surprisingly, as discussed

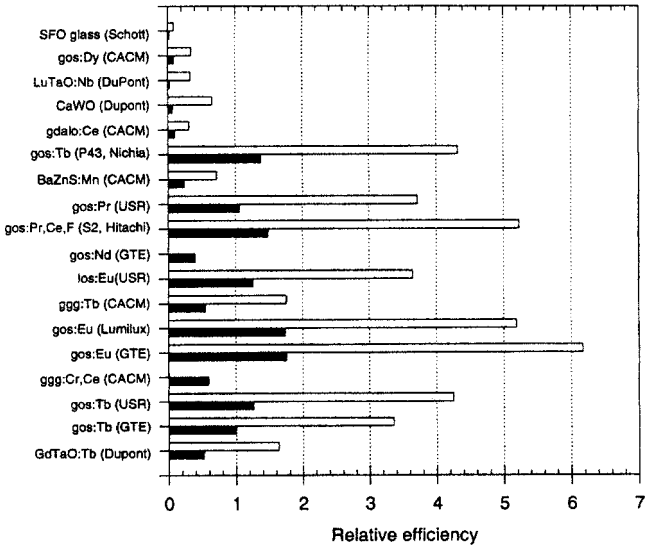

FIG. 4. The efficiency of the phosphor is greatly improved by coupling to back-illuminated CCDs (open bars), rather than front-illuminated CCDs (filled bars) (Ref. 33).

below, optimum resolution is not always achieved by eliminating the void volume.

Structured phosphor screens and scintillating fiber optics are alternative ways of increasing stopping power while preserving resolution—see Sec. II B 1 8 on spatial resolution.

3. Spectral matching. The detector efficiency depends on the spectral matching of the luminescence to successive elements of the light relay (Fig. 1). In general, photocathodes of image intensifiers have peak responses toward the blue. CCDs are available in front-illuminated and back-illuminated[52] forms. The most common front-illuminated CCDs are relatively insensitive in the blue end of the spectrum. Back-illuminated CCDs are much more expensive than their front-illuminated counterparts, with the consequence that their use is limited. Figure 4 illustrates the large increases in efficiency when coupling to back-illuminated CCDs. Recently, Kodak has introduced front-illuminated CCDs with electrodes that are more transparent in the blue, thereby enhancing blue sensitivity.[53]

A less important, but not insignificant additional spectral matching concern has to do with transmission through the optics which couple the phosphor screen to successive relay elements. Many phosphors have part of their emission in the near ultraviolet (UV), where glass transmission starts to fall. Another coupling consideration is that coupling fiber optics have a higher numerical aperture in the red, due to an increase of the critical angle of reflection at longer wavelengths. This can result in a significant enhancement in the light captured and conveyed through the fiber optics (see Fig. 11).[54]

Spectral matching considerations may be subtle. A good example is given by Gd_2O_2S:Tb, one of the most important x-ray phosphors.[33] Many of the major phosphor manufacturers list several Gd_2O_2S:Tb phosphors under different product numbers, depending on whether the phosphor is optimized for a cathode ray tube or x-ray applications. The specific manufacturing differences between the phosphors (e.g., dopant concentrations, particle sizes, and particle finishes) are often proprietary and not fully described in the product description. The luminescence arises from the Tb^{+3} center and is due to transitions between $^5D_4-^7F_J$ levels, mainly in the green, and $^5D_3-^7F_J$ levels, mostly in the blue. The relative excitations between these two level systems are a function of the Tb dopant concentration, with lower concentrations yielding more luminescence in the blue. ''X-ray phosphors'' are typically used in radiological applications to either enhance the sensitivity of x-ray film or to couple to x-ray image intensifier photocathodes, both of which are blue sensitive detectors. Hence, as far as most phosphor manufacturers are concerned, an ''x-ray phosphor'' should be optimized for maximum blue emission. On the other hand, the cathode ray tube and lamp variants tend to be enhanced in the green to better match the peak spectral sensitivity of the eye. Gd_2O_2S:Tb is now often used in detectors in which the phosphor is directly coupled via fiber optics to a CCD. In this case, both the fiber optics and the CCD are more effectively coupled in the green than the blue, so using the material listed as an x-ray phosphor is exactly the wrong thing to do!

4. Energy efficiency. Energy efficiency refers to the fraction of the stopped x-ray energy that is emitted as light. Robbins[55] has shown that the maximum energy efficiency n is given by

$$n = h\nu_e / E, \tag{2.1}$$

where h is Planck's constant, υ_e is the averaged frequency of luminescent radiation, and E is the average energy required to create an electron-hole pair. E varies from about three times the band gap for NaI and CsI to about seven for $CaWO_4$, and is dependent on the band gap, the high frequency and static dielectric constants, and the frequency of the longitudinal optical vibration mode. High efficiencies result if the optical vibrational modes are of low frequency and the emission energy is close to the band gap energy. Energy efficiencies (i.e., the fraction of the stopped x-ray energy which is emitted as luminescence) range down from about 20% for ZnS:Ag. Gd_2O_2S:Tb is about 13% efficient and $CaWO_4$ is about 6.5% efficient.[56,57] A consequence of Eq. (2.1) is that x-ray phosphors, which are dramatically much more energy efficient than ZnS:Ag, are unlikely. It should be noted that it is very difficult to measure the absolute energy efficiency of a phosphor. Further, the efficiency is a function of the exact phosphor composition and synthesis procedure, the grain size, the grain surface treatment, etc., with the result that energy efficiency values in the literature[55–60] vary considerably.

Note that the detailed mechanism of electronic excitation, and, hence the energy efficiency, may be different for UV and the very energetic photoelectrons produced by highly ionizing radiation.

5. Luminescence decay time and afterglow. Luminescent decay refers to the way the intensity of luminescent emission decreases with time after excitation. Measurement of phosphor screen decay times in the context of x-ray detectors is difficult, but important.[32,33,40,60,61] Ideally, the phosphor luminescence decays exponentially with a short time constant. Unfortunately, in real phosphors the decay curve (Fig. 5)

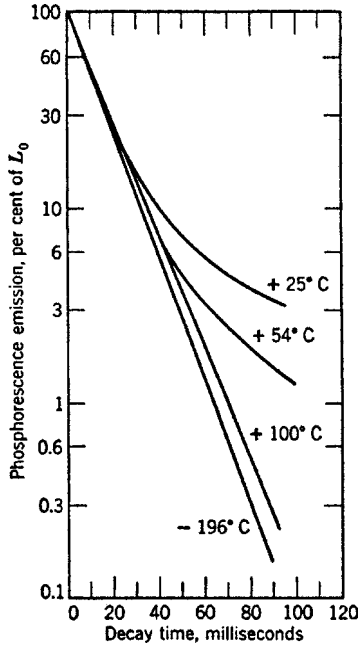

FIG. 5. The luminescent emission of a phosphor ideally decreases exponentially with time. At some time, the luminescent decay from most phosphors switches from exponential to a slower algebraic form. In this example, algebraic decay is observed at intermediate temperatures for rbhdl.-Zn_2SiO_4:Mn(0.3) (Ref. 14).

generally divides into two regimes: prompt decay and afterglow, the latter also being known as persistence. The prompt decay is an initial, typically exponential decrease of intensity with time and is due to the primary radiative process. Cases in which the exponential decay dominates for three or four decades of luminescent intensity are rare. More commonly, after one or two decades of decay, the luminescence is characterized by an algebraic decrease of the form

$$I(t)=t^{-\mu}. \tag{2.2}$$

I is the intensity of luminescence, t is the time, and μ is generally less than 2. The afterglow is due to trapping phenomena which is complex and often not understood. Frequently, a complicated temperature dependence is observed.[14] Figure 5 illustrates that the interplay between temperature and persistence can be very complex.

Persistence limits the rate at which a rapidly changing x-ray image may be recorded. The problem increases with the desired dynamic range of the data. Consider, for example, the acquisition of diffraction patterns of a crystal being rotated in an x-ray beam. Diffraction spots appear, brighten, and then disappear, all in less than a few tenths of a degree of crystal rotation; furthermore, nearby spots in the diffraction pattern may differ in intensity by several orders of magnitude. Imagine a weak spot that appears in nearly the same position on the detector as where a very bright spot had just appeared. It is desirable for the afterglow of the bright spot to have decayed by at least four orders of magnitude by the time the weak spot appears. At an intense synchrotron radiation source, the rate of crystal rotation may be very rapid and the time between appearance of the spots may be a few tenths of a second. Most phosphors will not decay by four orders of magnitude in this short time. The algebraic nature of persistence also may lead to a slow buildup of background intensity due to the ever-present low level of diffuse background between the Bragg spots. In consequence, as time progresses, it becomes increasingly difficult to accurately measure very weak spots because of rising background levels.

Some materials have traps which are too deep to be thermally excited in short amounts of time. These traps may become excited and luminesce upon x-ray exposure. The result is a ghost image of the last x-ray image taken superimposed on the diffuse background of a new image. In some cases, the trapped ghost images may be stored indefinitely only to reappear upon further x-ray exposure. In other cases, shallower traps may be populated which may be optically photoexcited into luminescence. Such ''storage phosphors'' have recently found important applications as x-ray detectors (also called ''image plate detectors'').[62–68] The phosphor is exposed to acquire the x-ray image and then later read out by scanning the phosphor with a laser to excite the traps into luminescent emission, which is detected by a photomultiplier. The most important example of such a storage phosphor is BaFBr:Eu^{2+}, which may be photoexcited with red HeNe laser light.

6. Linearity of light output. The output light intensity of a phosphor will vary nonlinearly with the input x-ray intensity if there is significant ground state depletion of the activator and certain trapping phenomena. Excited state absorption and Auger processes may also result in nonlinearity effects.[12] Phosphor saturation effects have mainly been investigated in cathode ray tube applications where the specific energy doses are very high, both because of large electron currents incident over very small phosphor screen areas and because the electrons do not penetrate deeply into the phosphor, thereby yielding most of their energy in a thin phosphor layer. By contrast, typical x-ray energy doses have been very much smaller than electron energy doses, especially in cases where one requires a large dynamic range of intensity linearity in the x-ray signal, with the consequence that few intensity linearity studies have been performed. However, very high specific x-ray intensities are now obtainable with synchrotron radiation sources. This makes detailed investigation of the linearity of x-ray phosphors over a very wide range of x-ray intensities feasible; indeed, synchrotron radiation applications are likely to necessitate such studies.

Whereas intensity linearity refers to light output as a function of the rate of incident x-ray energy, dose linearity refers to the light output per unit x-ray input as a function of the total integrated incident x-ray exposure. Nonlinearity with respect to dose means the phosphor is changing and, most typically, is suffering radiation damage. The inorganic phosphors in Table I are generally very radiation hard and can sustain enormous doses without significant damage, as may be seen by considering the doses on cathode ray tubes; a modest cathode ray tube electron beam of, say 1 μA and 30 kV potential delivers the same energy dose as about 10^{13} 15 keV x rays into a very small volume of phosphor. This is comparable to the most intense monochromatic beams available at modern synchrotron x-ray sources. Although cathode ray tubes do eventually suffer from burn-in, this is typically

only after very long periods of exposure (months or years).

Many phosphor screens consist of micron-sized phosphor grains held together by a binding material, such as an organic polymer. Organic materials are much more susceptible to bond scission and degradation, with the result that the first sign of radiation damage may be a breakdown of the binding matrix, leading to flaking or discoloration of the phosphor screen. Inorganic binders, such as silicates,[44,45] are somewhat more robust. However, even with typical organic binders, one needs enormous doses before damage is evident.

7. Noise. Phosphor noise arises from statistical variations in the light output per incident x ray. In high-gain photon counting detectors, it is frequently possible to set a discrimination threshold such that the counting statistics are dominated by the shot noise of the incident signal and the stopping power of the phosphor. The statistics are more complex in integrating detectors, where the light from a given patch of phosphor screen is integrated before being read out. Assuming a Poisson x-ray source, the output signal-to-noise ratio (SNR) of the phosphor is given by

$$\mathrm{SNR}=(N_0A_QI)^{1/2}=(N_0A_N)^{1/2}, \tag{2.3}$$

where N_0 is the number of incident x-ray photons in the integration time and area, A_Q is the quantum absorption of the phosphor screen, I is a factor between 0 and 1, and $A_N=A_QI$ is called the noise-equivalent absorption.[69–71] If each stopped x ray yielded the same light output, then $I=1$ and the SNR is simply dominated by the incident quantum statistics and, importantly, the fraction of x rays stopped. Swank[69] has shown that

$$I=M_1^2/M_0M_2, \tag{2.4}$$

where M_i are the ith moments of the scintillation pulse-height distribution. $I\cong 1$ if the pulse-height distribution is very sharply peaked.

Factors that lead to light output fluctuations *per stopped x-ray* result in values of I less than unity, e.g., $A_N<A_Q$. Swank[69] identifies three such factors: the distribution in incident x-ray energies, intrinsic variations in the number of photons produced per x ray at a given energy, and light output variations resulting from light collection efficiency considerations. The first factor simply results from the fact that the lower energy x rays of a polychromatic x-ray source yield less light. Intrinsic variations occur because of a stochastic distribution of the stopped x-ray energy into channels that do not result in light output. For example, at x-ray energies just above a K absorption edge of the phosphor, x-ray fluorescence can cause much of the stopped energy to escape the phosphor in the form of low energy x rays. Fluctuations in the light collection efficiency result, e.g., when the phosphor screen is not totally transparent to the emitted light; more light will be collected from x rays which are stopped closer to the side of the phosphor screen facing the optical detector than those stopped further from this side. Swank[69] has calculated A_N for several x-ray phosphors.

The phosphor limits the performance of the detector in fundamental ways. As shown in Sec. IV F, the detective quantum efficiency (DQE), a measure of the overall detector sensitivity, has the stopping power of the phosphor as an upper limit. In other words, the performance of even an otherwise ideal, noiseless detector will not be optimal unless the phosphor stops all the incident x rays—this is intuitively obvious. What is not so obvious, is that the accurate measurement of an integrated signal is also limited by the system resolution. In so far as the phosphor is frequently the resolution-limiting element of the detector, it can degrade the accuracy of the desired measurement, even if the signal relay after the phosphor adds no additional noise. Thus, improvement of the phosphor stopping power, by increasing its thickness, usually degrades the spatial resolution, which also decreases the measurement accuracy of the system. For this reason, the compromise between phosphor stopping power and resolution must be carefully selected. Methods for choosing compromise values will be detailed in later sections.

8. Spatial resolution. The spatial resolution of a luminescent screen is determined by its ability to stop x rays through the thickness of the screen while minimizing the lateral spreading of the resultant light. Three kinds of scintillating screens are in use: screens of settled phosphor powders, single crystal screens, and microstructured screens. The spatial resolution of each of these screens is determined by different light propagation physics, as discussed below, in this section, and in the next section.

The resolution of a phosphor screen is characterized by the transfer function which maps the x-ray image into the output light image. Because the incident and output images are incoherent, it is sufficient to specify a real transfer function. The normalized point spread function (PSF),

$$1=\int_{x=-\infty}^{x=+\infty}\int_{y=-\infty}^{y=+\infty}\mathrm{PSF}(x,y)\,dx\,dy=2\pi\int_0^{\infty}\mathrm{PSF}(r)\,r\,dr \tag{2.5}$$

specifies the distribution in output signal for a point input signal, where the right-hand integral applies in the usual case of a uniform phosphor screen which is rotationally invariant about the screen normal.[72,73] Insofar as the phosphor may be approximated as linear in intensity response and stationary (e.g., the PSF is translationally invariant across the screen), then the output response, $h(x,y)$, to an input image, $g(x,y)$ is simply the convolution (represented by "*") of the PSF and the incident image

$$h(x,y)=\mathrm{PSF}(x,y)*g(x,y). \tag{2.6}$$

Other commonly used resolution measures are the modulation transfer function (MTF) which is the modulus of the Fourier transform of the line spread function (LSF), defined by

$$\mathrm{LSF}(x)=\int_{-\infty}^{+\infty}\mathrm{PSF}(x,y)\,dy. \tag{2.7}$$

As detailed in Sec. IV, detector noise, sensitivity, and resolution are related such that degradation of the resolution usually reduces the detector sensitivity. Phosphor screen optimization inevitably involves complex compromises between resolution and efficiency.[46,47,58,74,75] Since the x-ray phosphor is frequently the resolution-limiting element of the

detector, optimization of a detector involves full characterization of the phosphor screen resolution, i.e., measurement of the PSF out to at least several decades of intensity down from the peak response. Commonly used single-valued characterizations, such as the full width at half maximum (FWHM) of the PSF or the spatial frequency at which the MTF=5%, are insufficient.

This may be illustrated with an example of two screens of settled phosphor powder. The two screens differ only in that the void volume between the phosphor particles in one screen is filled with an index matching oil. In the absence of the oil, the very high index of refraction of the phosphor particles causes the path of the luminescent photons to bend sharply as the photons emerge from the phosphor into the adjacent void between the particles. The result is that the screen is strongly scattering and light photons execute a nearly diffusive, random walk in the screen. By contrast, the oil filled screen is more transparent. The oil filled screen has a sharper short-range PSF, as measured by the FWHM. This is a simple consequence of the fact that photons in a transparent screen have a mean free path that is long compared to the screen thickness, so the short-range PSF has a width comparable to the screen thickness. However, the long-range PSF of the transparent screen is wider than for the diffusive screen; in the transparent screen, photons directed nearly parallel to the surfaces travel a long distance before being scattered. In the diffusive screen the photons are constantly being redirected with a step size comparable to the phosphor grain width and so to diffuse a distance x must travel a path length that scales approximately as x^2. If the phosphor is not totally transparent to its own luminescence, as is typically the case, absorption limits the long-distance diffusion of light [Fig. 6(B)].[47] Thus, a properly settled powder screen often has a surprisingly good PSF, which accounts for its popularity (Fig. 7).

The overall light collection efficiency of a properly settled powder screen also often exceeds that of a screen with a transparent phosphor. The reason, again, has to do with the diffusive propagation of light in a settled screen: By Snell's law, light cannot enter the screen substrate if it is incident at too glancing an angle to the surface. In transparent phosphor layers, this reflected light can travel a long distance and be lost. In a diffusive screen, however, the nearly random-walk trajectory of the light means that the photons have a very high probability of returning to the substrate at a different angle and within a short distance from the initial point of refection. Thus, these photons have multiple opportunities to enter the substrate.

The efficiency of a phosphor screen can be enhanced by overcoating it with a reflective surface, such as an evaporated layer of aluminum or a thin glued-on layer of aluminized mylar, or depositing it directly onto the aluminized side of a mylar film.[47,58] This directs light that would otherwise be lost back into the phosphor. However, reflective layers also cause some loss of resolution, as the reflected light has a longer path length in the phosphor before hitting the substrate. In order to be effective, the reflective screen must be a good reflector, a situation which does not always apply to the rough surface of a settled screen.

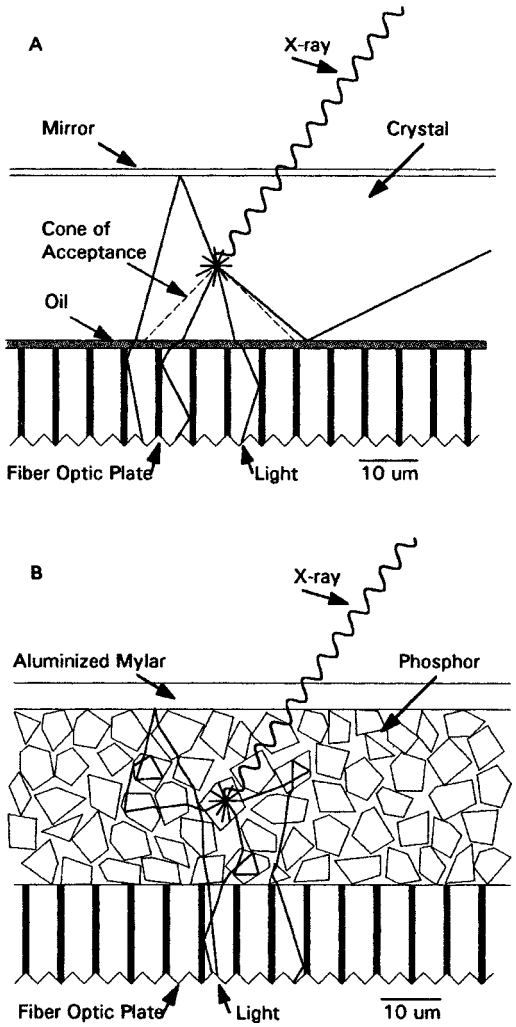

FIG. 6. Luminescent photons follow ballistic trajectories in clear, single crystal phosphor screens (A), but take an almost random walk in screens consisting of settled high index of refraction phosphor powders (B). The consequences are discussed in the text. [From Gruner *et al.* (Ref. 47).]

Long-range tails on the PSF have important consequences on the detector sensitivity for certain kinds of measurements, e.g., the measurement of resolution limited spots superimposed on a uniform x-ray background.

Measurement of the resolution of a phosphor screen typically involves the imposition of an x-ray shadow mask to create a known incident x-ray image, the luminescent image of which is then recorded and analyzed to determine the transfer function.[76] A mask of an x-ray opaque material containing a thin slit or a set of fine holes may be used, in conjunction with Eq. (2.5) or (2.7) to determine the short-range PSF. The analysis is most straightforward if the width of the slit or the diameter of the holes is small compared to the FWHM of the PSF. Otherwise it is necessary to deconvolute the hole via Eq. (2.6), a procedure that is difficult and susceptible to error if the holes are much larger than the PSF. Deconvolution procedures also require very high quality data and may be limited by Poisson noise in the signal, which, given the small size of the mask holes, necessitates very long x-ray exposures. Parallax artifacts may be eliminated by use of a small x-ray source at a distance and minimizing the distance between the mask and the phosphor. Since x rays

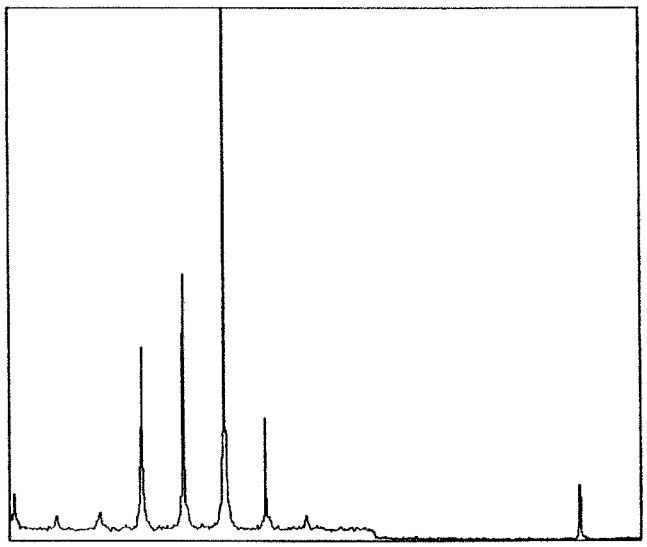

FIG. 7. A trace through a Laue diffraction pattern recorded with a settled phosphor screen fiber-optically coupled to a CCD with unity magnification shows the excellent resolution possible with a settled screen. A 20 μm diameter glass capillary was used to create a micro x-ray beam incident upon a gallium arsenide/gallium aluminum arsenide multiplayer. The FWHM values of the peaks are on the order of a single 27 μm CCD pixel. Reproduced from Eikenberry *et al.* (Ref. 164).

are penetrating, the masks are preferably of a dense metal (e.g., lead, gold, or tungsten) and the holes must be fabricated without a taper to the walls.

As an example, the mask we have used to determine the PSF of CCD detectors is a 10 cm$\times$10 cm, 50-μm-thick tungsten sheet with an array of lithographically fabricated 75-μm-diam holes on a 0.5-mm-square lattice.[76] In order to limit parallax, the x-ray source was a microfocus (0.2 mm spot size) x-ray tube at the end of a 1 m evacuated flight tube and the mask was placed within a few mm of the phosphor. The Gd_2O_2S:Tb phosphor screens being analyzed were designed for good stopping power in the 8–15 keV range, which translated to areal densities of about 10 mg of phosphor/cm^2. These screens were settled at roughly 40% bulk crystal density, corresponding to a thickness of about 30 μm. This sets a lower limit on the short-range PSF and suggested that a mask of 25-μm-diam holes would require no deconvolution. On the other hand, standard lithographic fabrication of precise holes in metals is most readily accomplished if the holes are at least as wide as the thickness of the metal. But 25-μm-thick sheet tungsten is not only fragile, it is slightly transparent to the high energy Bremsstrahlung x-ray background from the x-ray tube. The compromise was to use 75 μm holes in 50-μm-thick tungsten material, which necessitated some slight deconvolution. In addition, the x-ray tube was operated at a relatively low dc voltage of 10 keV, which was enough to excite the K_α line of the copper anode, but limited the production of higher energy Bremsstrahlung x rays.

Whereas the diffusive nature of light propagation dominates the light transmission through settled powder screens, the resolution of luminsescent screens made of single (or a few) crystals of scintillator is dominated by long-range scattering [Fig. 6(A)]. Arndt pointed out many years ago[77] that

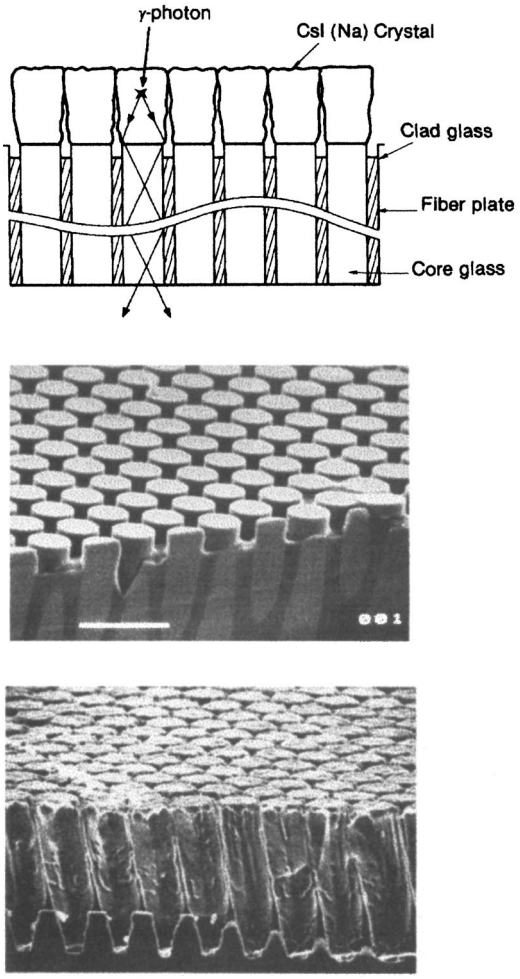

FIG. 8. CsI(Na) phosphor grown in columns on an etched fiber-optic plate (top panel). A micrograph of the plate before phosphor deposition, but after fiber matrix etching, is shown in the middle panel and after phosphor deposition in the bottom panel (Ref. 78).

lens coupling of a luminescent image through a transparent single crystal screen yields the highest short range PSF. Single crystal screens have recently been put to excellent use for microtomography applications,[37] in which a thin $Y_3Al_5O_{12}$:Ce crystal was lens coupled to a CCD camera to achieve 0.8 μm (FWHM) resolution.

Microfabricated screens utilize specifically microstructured luminescent materials in order to simultaneously enhance stopping power and spatial resolution, typically by fabricating the screen out of long, thin, ideally optically isolated columns of luminescent material. An approach that has been successfully used in x-ray image intensifier tubes is to grow CsI phosphor crystals in needlelike crystal habit.[38–41] The long phosphor needles grown perpendicularly to the substrate act similarly to optical fibers and guide the light to the substrate. More recently, textured substrates made of etched glass fiber-optic plates have been used to grow distinct columns of phosphor via evaporation[78,79] (Fig. 8). Another approach is to fabricate screens of an array of scintillating optical fibers. Scintillating fiber optics were first suggested by Reynolds[80] many years ago for high energy physics applications. More recently, scintillating fiber-optic glass plates have been developed.[81–87] As will be discussed

in the section on fiber optics, the technology of high spatial resolution fused fiber-optic glass plates is sophisticated. By comparison, relatively little work has been done on fused scintillating glass fiber optics, so there is certainly much room for improvements in the overall efficiency and resolution of scintillating fiber optics. A final alternative is to fabricate a plate consisting of an array of parallel hollow holes by etching out the cores of fused glass fiber-optic plates or by other lithographic methods. These may then be filled with phosphor grains[88] or by evaporation or by solution deposition of phosphor.[42] Ideally, the inner walls of the plate are coated with reflective gold to optically isolate the columns, although, in practice, it is very difficult to provide an adequate coating along the full length of long aspect ratio holes. Another difficulty with this approach is that the walls of the matrix separating the phosphor columns do not luminesce and, therefore, the fill factor of the screen is less than 100%.

The discussion, above, has been oriented toward light emitting phosphors. However, phosphors can also be used as photocathodes. Indeed, porous, mossy CsI photocathodes under high electrical potentials can have significant electron gain[89] and have been used in experimental x-ray image intensifiers.[90]

2. Semiconductors

The semiconductors out of which CCDs are made may also be used to directly convert x rays to electron-hole pairs, thereby avoiding the many problems associated with phosphors and light collection. CCDs made of standard, low resistivity silicon have active charge-collecting depletion regions that are only a few microns thick, which severely limits the efficiency of direct x-ray conversion. The alternative is to make deep depletion CCDs out of high resistivity silicon or, even better, higher stopping power semiconductors. Since efficient direct-conversion CCDs generally need to be custom fabricated, it is often as practical to also consider other custom fabricated direct conversion architectures, such as diode arrays and pixel array detectors. An understanding of the physics of x-ray conversion in semiconductors is required in order to evaluate whether a CCD or alternative semiconductor architecture best meets a given need. For this reason, the sections on semiconductors summarize the general physics of x-ray conversion.

Studies in the early part of the 20th century established that certain crystals conduct electricity when exposed to radiation. Early work was plagued by the lack of well-understood, well-characterized materials. The situation began to change in the 1940's with better understanding and availability of good quality semiconductor materials (e.g., see Coche and Bertolini[91] for a brief history). Throughout the middle third of the 20th century, semiconductor detectors were developed primarily as single, or a few, element energy resolving detectors for radiation spectroscopy. The development of semiconductors for multielement detector arrays had to await the development of lithographic fabrication technology developed during the last third of the 20th century. Recent developments have also been aided by the expertise and technology developed for the semiconductor electronics industry. Semiconductor x-ray converters may be expected to increasingly supplant phosphors.

Semiconductor converters have significant advantages over phosphors: Semiconductors directly convert the x-ray energy into electrical charge, which often simplifies the design of the detector. The physics of x-ray absorption and electron-hole production in a semiconductor is generally simpler and, therefore, better understood than light production in phosphors. Compared to phosphor converters, semiconductors are also usually much more efficient, resulting in more charge carriers, are more linear and less noisy, and the charges are more rapidly and more efficiently collected. The disadvantages of semiconductors that have limited their use as x-ray converters is that large area semiconductor screens are difficult to fabricate, thick detectors are hard to make, and the semiconductor of choice, namely silicon, has relatively low stopping power.

Excellent descriptions of the physics of semiconductor detectors may be found in Bertolini and Coche[91] and Dearnaley and Northrop[92] and in course notes posted by Spieler.[93] The process begins with the photoabsorption or Compton scattering of the x ray in the material. Within about a nanosecond the emitted electrons cascade through an energy degradation process resulting in many electron-hole pairs. This occurs in a very localized region since the range of low energy electrons is quite short in most materials, and may be approximated by

$$\begin{aligned} R &= 0.090\rho^{-0.8}E^{1.3} \quad \text{for } E<10 \text{ keV}, \\ R &= 0.045\rho^{-0.9}E^{1.7} \quad \text{for } E>10 \text{ keV}, \end{aligned} \tag{2.8}$$

where R (microns) is the thickness of material to reduce the electron transmission to 1%, E is the electron kinetic energy (keV), and ρ is the material density ($\mathrm{g\,cm^{-3}}$).[94] For silicon, this translates into a range of about a micron for 10 keV x rays, which affords excellent intrinsic spatial resolution. The mean ionization energy to produce an electron-hole pair ε determines the average number of electron-hole pairs produced, N_{eh}, as

$$N_{\mathrm{eh}} = E/\varepsilon, \tag{2.9}$$

where E may be taken to refer to the x-ray energy. Since ε typically is a few eV, many electron-hole pairs are produced. Furthermore, the fractional variation, $\sigma(N_{\mathrm{eh}})/N_{\mathrm{eh}}$, in the number produced is quite small because the energy degradation process offers few channels which do not lead to electron-hole pairs:

$$\sigma(N_{\mathrm{eh}})/N_{\mathrm{eh}} = \sigma(E)/E = \sqrt{(F\varepsilon/E)} = \sqrt{(F/N_{\mathrm{eh}})}, \tag{2.10}$$

where F is an empirical factor known as the Fano factor.[91] For silicon, $F \approx 0.1$. The fact that the Fano factor is small ultimately accounts for why semiconductor detectors have excellent energy resolution.

The ionization energy E_{ion} is related to the energy band gap of the material E_{gap} and is approximately given in eV by Klein's empirical formula[95]

$$E_{\mathrm{ion}} = 2.67E_{\mathrm{gap}} + 0.87. \tag{2.11}$$

See Sec. II. Note, incidentally, that better, measured values for E_{ion} for silicon are 3.62 to 3.65 eV. See Table II.

The electron-hole pairs rapidly recombine unless they are swept apart by the presence of an electric field, such as is normally present in the depletion zone of a reverse-biased semiconductor diode. The behavior of electrons and holes in the depletion zone are the primary determinants of the x-ray detecting characteristics of the semiconductor. The depletion zone is either (1) of the surface barrier type, which forms at the junction of a semiconductor and a suitable metal, or (2) of n-p type, which forms at the junction of n- and p-doped semiconductor materials. What follows is a simplified description of a p-n detector. More detail on both types of junctions may be found in Bertolini and Coche.[91]

Imagine a junction between n- and p-doped material. Initially each material is charge neutral, the main difference between them being that the n-type material effectively has only electrons as mobile charge carriers with the charge-compensating holes fixed in the lattice, while the p-type material is the other way around. The mobile carriers may be considered to be a kind of gas of charged particles diffusing about fixed counterparts of the opposite electrical sign. When the two types of material are brought into contact at room temperature, the electrons diffuse across the junction into the p material and the holes diffuse across into the n material. In doing so, however, charge neutrality in each material is violated. The p material now has a surplus of electrons and the n material a surplus of holes, thereby creating an electric field which points from n to the p material. At equilibrium, the electric field strength is sufficient to prevent further net separation of holes and electrons. Call the resultant net potential across the junction V_0; it is a function of the temperature and the properties of the materials. A consequence of the field is that any mobile charges introduced into the field region are swept, depending on their sign, toward one end or another of the region; hence, the region is depleted of free charge carriers and is known as the depletion zone. Since the depletion zone has no free charge carriers, it effectively is an insulating gap. It is readily shown that the width of the depletion zone is given by

$$x=\left[\frac{2\varepsilon V_0}{e}\,\frac{(N_a+N_d)}{N_aN_d}\right]^{1/2}, \tag{2.12}$$

where ε is the semiconductor dielectric constant, e is the magnitude of charge of the electron, and N_a and N_d are the bulk concentrations of acceptor and donor dopants in the p- and n-type materials, respectively.

If the n and p sides of the junction are now connected to the positive and negative terminals, respectively, of a battery then there is an additional component of electric field across the junction that adds to the contact field, displaces the equilibrium separation of charge, and expands the width of the depletion zone. The junction is now reverse biased. Typically, one material, say the p type, is much more heavily doped than the other, in which case $N_a \gg N_d$, and the imposed potential $V \gg V_o$. In this case, it can be shown that

$$x \approx \sqrt{2\varepsilon\mu_n\rho_n V}, \tag{2.13}$$

where μ_n is the electron mobility and ρ_n is the resistivity of the n-type material. Consequently, for a thick depletion zone, which is desired for an x-ray detector, one needs some combination of a high, imposed potential, high resistivity, or high electron mobility. An analogous equation holds if the n-type material is more heavily doped.

If an x ray stops in the depletion zone the electron hole pairs that are created are swept to the respective ends of the diode and appear as a current pulse. Since the number of electron-hole pairs is ideally proportional to the x-ray energy, the charge of the pulse is proportional to the x-ray energy.

In order to be useful as a quantitative x-ray converter, the semiconductor detector should ideally meet many constraints:

(1) The width of the material between the depletion zone and the incident x rays should be thin, since x rays that are stopped in these regions do not contribute to the signal.
(2) The depletion zone should be thick enough to stop practically all the x rays. Because of stopping power considerations, high atomic weight semiconductors become increasingly attractive at higher x-ray energies. In view of Eq. (2.13), this suggests that the semiconductor resistivity should be high. The imposed voltage is limited by breakdown considerations.
(3) The rate of loss of the dominant signal carriers (i.e., electrons in the above example) should be low. Carriers may be lost through recombination or trapping.
(4) Spontaneous generation of electron-hole pairs should be low, since these constitute a dark current in the absence of x rays. Electron-hole pairs may be created thermally or at various defects, especially at the interfaces of the device.
(5) The junction capacitance should be as low as possible, since, in general, the performance of the charge sensitive preamplifier connected to the detector degrades with increasing input capacitance. This argues for a thick depletion layer.
(6) The Fano factor of the semiconductor should be as low as possible for low noise performance.
(7) The detector should be robust, stable, of adequate size, etc. Most importantly, good quality semiconductor material, and the techniques to fabricate it, must be available.

Not surprisingly, the availability of a high quality semiconductor is directly linked to its use by the electronics industry. Silicon is nearly ideal in all respects except for stopping power considerations (Fig. 9 and Table II). The attenuation length of Si rises from 130 μm at 10 keV to 1038 μm at 20 keV. Germanium and gallium arsenide are both still effective at 20 keV, but large area, high quality, high resistivity materials are more difficult to obtain than with silicon. Although CCDs have been fabricated out of other semiconductors,[96] practically all commercially available CCDs are made of silicon. This situation is different for other sensor architectures, such as diode arrays, in which the diode layer fabrication is simpler than for CCDs. Alternative sensors arrays are discussed at the end of this review.

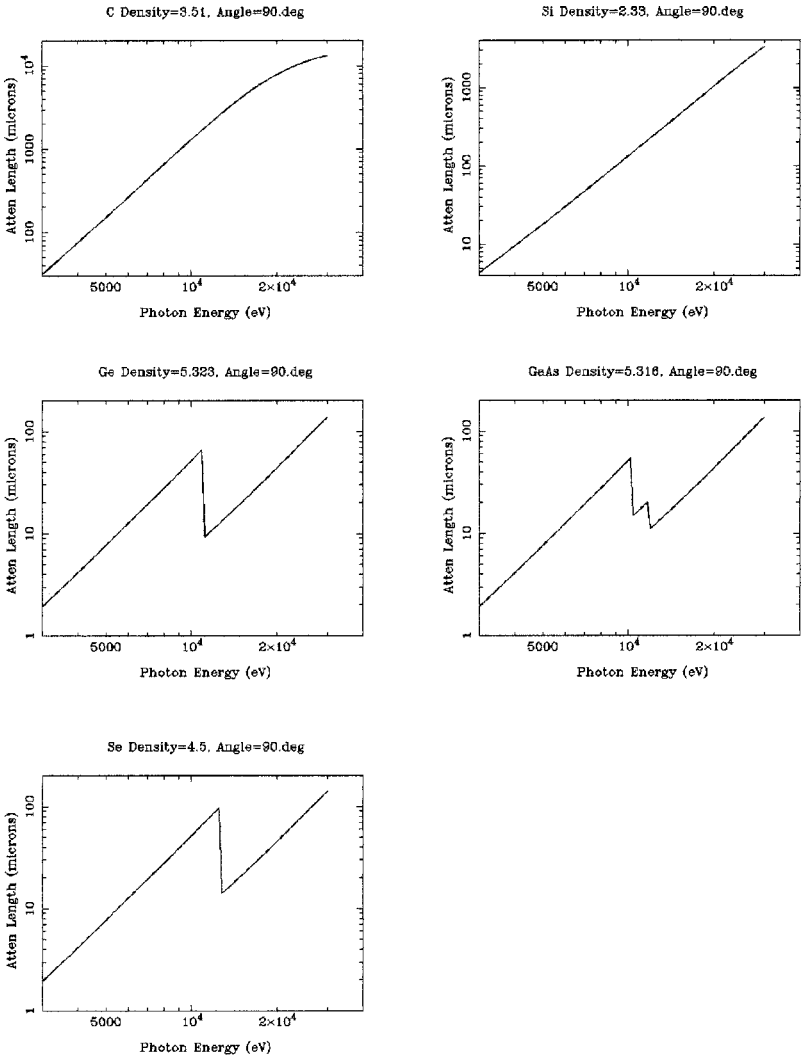

FIG. 9. Attenuation lengths are shown for the semiconductors of Table II. These figures were produced with the on-line calculator at http://www-cxro.lbl.gov/optical_constants/atten2.html

C. Optical coupling methods

Optical couplings are often required to connect elements of the signal relay of Fig. 1. Optical couplings may be done via proximity coupling, lenses, and fused fiber optics.

1. Proximity coupling

Proximity coupling simply involves keeping the distance between successive optical elements as small as possible. For example, in the large area x-ray intensifiers used for radiology, the phosphor is deposited on the internal (vacuum) side of the x-ray entrance window and the photocathode is directly deposited onto the phosphor. CCD detectors may also use phosphors directly deposited onto the CCD.[79,97,98] Proximity coupling may be efficient, but it limits the use of commercially available modular components and does not allow a change of magnification of the coupled image, such as is possible with lenses and fused fiber optics.

2. Lens coupling

Lens coupling is simple and convenient, but often unacceptably inefficient. The efficiency C of lens coupling an image, purely from solid angle considerations, is given by

$$C=[M/\{2\,f(1+M)\}]^2, \tag{2.14}$$

where the magnification M is the ratio of the sizes of the image to the object, and f is the "f number" of the lens, i.e., the ratio of the focal length to the lens diameter. The efficiency given by Eq. (2.15) is listed in Table III for a $f/1.0$

TABLE II. Values of E_{gap} for some semiconductors of interest.

Semiconductor	E_{gap} (eV) at 300 K
C (diamond)	5.5
Si	1.12
Ge	0.67
GaAs	1.45
Gray Se	1.8

TABLE III. Efficiency of $f/1.0$ lens and fiber optic tapers at various magnifications.

Magnification (image size/object size)	$f/1.0$ lens efficiency (%)	Fiber optic taper efficiency (%)
1	6	75
0.5	3	20
0.3	1.3	13
0.25	1	9

lens; it is seen that the efficiency falls rapidly if the object has to be demagnified. Unfortunately, it is frequently required to couple a large area phosphor to smaller intensifiers or CCDs. Moreover, since the number of visible photons/x ray produced in the phosphor is very limited, this coupling has to be done as efficiently as possible.

The situation is very different if the x-ray image can be magnified, in which case lens coupling is often the simplest and most effective means of coupling. Magnification of the image can be done efficiently because, in this case, the lens can subtend a very large solid angle relative to the luminescent screen. This is, of course, the basis of microscopy. An example of an application where magnified lens coupling serves well is microtomography, in which the x-ray image may be only a small fraction of a millimeter across.[37,99,100]

3. Fiber optics coupling

In demagnifying geometries fused fiber optics are generally more efficient than lenses (Table III). A fused fiber-optic bundle, henceforth to be simply called fiber optics, consists of a coherent bundle of glass-fiber light guides, each fiber being, say, 10 μm or so in diameter. The bundle may be heated until the glass softens and is stretched so as to produce a fiber-optic taper to magnify or demagnify an image. Modern fiber optics approach the theoretical limit of demagnification efficiency imposed by solid angle considerations and Snell's law (see Fig. 11 and Coleman[54]).

A numerical example will illustrate why fiber optics are often required. In general, the response of the signal chain of Fig. 1 to a detected x ray is given by

$$N_S = N_P C_{PI} G_{PP} C_{IS} Q_S, \tag{2.15}$$

where N_S is the number of quanta in the image sensor, say electrons in the CCD, N_P is the net number of visible light photons/x-ray emitted from the phosphor towards the gain element, say an intensifier, C_{PI} and C_{IS} are the efficiencies with which quanta are conveyed from the phosphor to the intensifier and from the intensifier to the sensor, G_{PP} is the photon gain of the intensifier, and Q_S is the quantum efficiency of the sensor to the intensifier output.

Some best case numbers are useful in evaluating Eq. (2.15): efficient x-ray phosphors, such as Gd_2O_2S:Tb, convert about 15% of the x-ray energy to light (see Table I). Given that many of these photons are emitted in the wrong direction, even with reflective coatings over the phosphor, one is doing very well if 10% of the energy can be directed toward the intensifier. For an 8 keV Cu K_α x-ray and light emission of 2.5 eV photons, this corresponds to about 320 light photons. The efficiency of coupling an image depends on the magnification ratio and whether the coupling is done via lenses or fused fiber-optic bundles (see Table III). Front-illuminated CCDs have quantum efficiencies of about 30%. Finally, as a benchmark we want the integrated signal to exceed the CCD noise. The signal-to-noise ratio will depend on the area being integrated and specifics about the CCD, but for our example, assume that the detector PSF is extremely sharp and single pixel performance is needed. This assumption is, in fact, overly stringent for most systems, but serves for comparative estimation. Scientific CCDs operated in slow scan mode with commercial controllers have about ten electrons noise per pixel.

For simplicity, let's first examine the case of directly coupling a phosphor to a front-illuminated CCD without intervening intensification. The most efficient way of optically coupling a phosphor to a CCD is to directly deposit it onto the CCD, i.e., a 1:1 area coupling. This corresponds to $(C_{PI} G_{PP} C_{IS}) = 1$. Hence, the signal per pixel, is $320 \times 1 \times 0.3 = 96$ electrons, comfortably above the 10 electrons noise per pixel for a S/N ratio of almost 10.

Next, consider the case of demagnifying the phosphor image onto a CCD via a magnification of 0.3 and without image intensification. This is not unusual, since CCDs larger than 2 or 3 cm across are difficult to obtain and one often wishes to have x-ray sensitive areas at least 6–9 cm across. Referring to Table III, we see that the efficiency of coupling with a $f/1.0$ lens, is only about 1.3%. The average signal is now $320 \times 1 \times 0.013 \times 0.3 = 1.2$ electrons/x ray, yielding S/N ≈ 0.1. On the other hand, if a fiber-optic taper is used, the coupling efficiency is 13%, which is about seven times better than lens coupling. The signal is now $320 \times 1 \times 0.13 \times 0.3 = 12.4$, or S/N$\approx 1$, which is much more acceptable.

Lens coupling inefficiencies might be acceptable after a gain element, such as an intensifier, where there are many more signal quanta, or, as noted in the previous section, when the luminescent image must be magnified. However, lenses, more so than fiber optics, limit the ultimate contrast of small features due to reflections and imperfections at the air–lens interface.[101] To limit these effects, the lens surfaces must be coated with antireflection films and kept meticulously clean. This is often more difficult than it might seem since volatile oils are ever present in laboratories and have a way of forming foggy films on glass surfaces, necessitating hermetic enclosures. By contrast, fiber-optic surfaces are usually coupled with thin layers of optical coupling gels or epoxy. Although these have to be applied in clean environments, once applied, they are effectively self-sealing against dust and dirt.

1. Fiber optics characteristics. Fused fiber-optics technology is reviewed by Siegmund.[102] Additional useful information may be found in product guides from Schott Fiber Optics and Incom fiber optics, two major U.S. fused fiber optics manufacturers.[103,104] Attention to detail is essential if fiber optics are to perform well, and x-ray detection needs push the state of the art. Key characteristics that have to be considered include

(a) numerical aperture;
(b) fiber size and bundle size;
(c) extra mural absorption (EMA);
(d) core to cladding ratio;
(e) shears, defects, and gross distortion; and
(f) actinide contamination.

We first summarize these characteristics and then describe tests to characterize fiber-optics parts in Sec. II C 3 2.

A single fiber in a fused fiber optic bundle consists of a core glass of high index of refraction N_C, surrounded by a

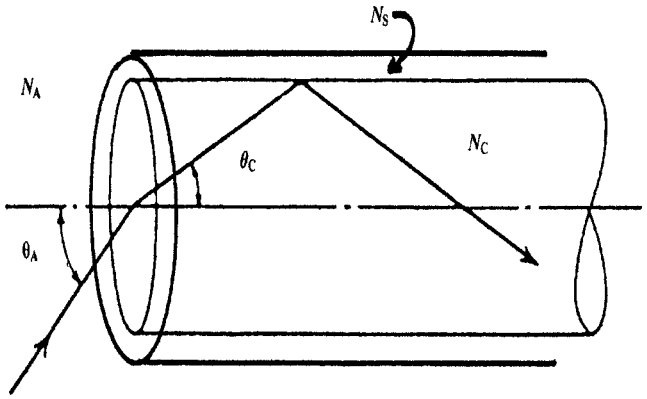

FIG. 10. An optical fiber of index of refraction, N_C, and cladding of index N_S, will accept incident light from a material of index N_A according to Snell's Law: $N_A \sin \theta_A = N_C \sin \theta_C$. Light will propagate down the fiber provided there is total internal reflection at the cladding-core interface.

lower index (N_S) glass cladding (Fig. 10). By Snell's law, light incident upon the core from a material of index N_A will propagate along the fiber by total internal reflection as long as the angle of incidence to the core is less than $\theta_A = \theta_{\max}$, given by

$$N_A \sin \theta_{\max} = (N_C^2 - N_S^2)^{1/2}. \tag{2.16}$$

The numerical aperture (NA) is the sine of the half-angle of the acceptance cone and simply equals $\sin \theta_{\max}$ when the incident medium is air, i.e., when $N_A \approx 1$. A NA=1 fiber plate, which is a standard fiber optic product, will propagate some light even when the light is incident at entrance angles almost parallel to the plate surface. Not all light is accepted even for NA=1 fibers, however, due to reflective (Fresnel) losses as the incident angle approaches 90°. Still, this 2π steradian acceptance cone is why NA=1 fiber optics are so efficient relative to lenses. Note that the indices of refraction, and hence the efficiency of transmission, are dependent upon the wavelength of the light.[54] The fiber transmits red light more efficiently (Fig. 11).

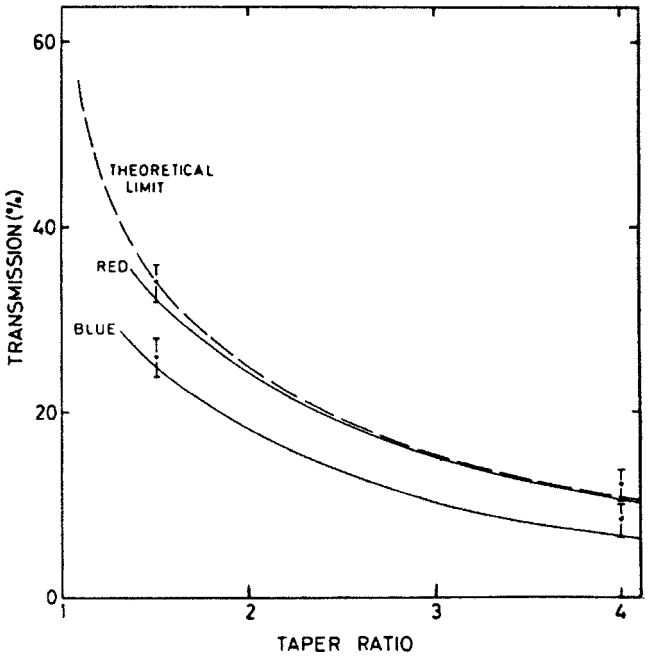

FIG. 11. The measured light transmitting efficiency of fiber-optic tapers compared to the theoretically expected values for red light versus the taper ratio. A taper ratio of 4 corresponds to a demagnification of a factor of 4. The difference in transmission between red and blue light is a consequence of the wavelength dependence of the indices of refraction in the glass components. Reproduced from Coleman (Ref. 54).

For tapered fibers,

$$d_{\text{small}} \sin \theta_{\max,\text{small}} = d_{\text{large}} \sin \theta_{\max,\text{large}}, \tag{2.17}$$

where d refers to the fiber diameter and "small" and "large" refer to the respective ends of the fiber. Equation (2.17) describes the divergence of light propagating down a reducing fiber. Since the NA will still be governed by Eq. (2.16), some of the uncollimated light entering the large end of the fiber will exceed the maximum allowed angle and be lost enroute to the small end.

Typical fiber sizes range from about 3 to 25 μm. The fiber size directly determines the resolution of the bundle. However, transmission losses rise as the fiber size decreases towards a few microns; this is a major consideration limiting the size of fibers on the small end of the fiber-optic taper. In the usual process, fibers are drawn and then cut into lengths which are stacked into a cane of square or hexagonal cross section, which is itself then fused, drawn, cut into lengths, stacked, and fused into a large boule or bundle. The size of the boule determines the ultimate size of the fiber-optic part. Parts greater than 15 cm across are available.

Some light always leaks out of the fibers due to scattering and imperfections. Large light losses also are expected in reducing tapers. Stray light can lead to "cross-talk" between fibers unless it is removed. For this reason, fiber optics are available with interspersed black absorbing glass, called EMA, which serves to absorb stray light. EMA can consist of tiny fibers stacked into the interstices of the regular fibers, a black cladding around the fibers, or a sparse substitution of occasional black fibers for transmitting fibers. Fiber optics without effective EMA is of very little use in high-resolution x-ray detectors.

The core to cladding ratio is the ratio of the cross-sectional areas of the core and cladding. Since light incident upon the cladding of a fiber-optic plate is not propagated (it, in fact, contributes to stray light), the core to cladding ratio sets an upper limit on the fraction of incident light that will be transmitted. The natural mismatch between core and cladding of two butted fiber optic plates accounts for most of the inefficiency of fiber optic to fiber-optic couplings.

The fusing and drawing involved in producing fiber-optic boules and parts introduces distortions and defects. Fibers at cane edges get flattened and distorted, leading to a visible hexagonal or square mesh known as "chicken wire." This comes from the reduced transmission of the flattened fibers. Fibers also break and small inclusions of gas or dirt lead to point blemishes where light transmission is reduced or blocked. Plastic distortion when the canes are fused leads to discontinuous breaks, called shears, between the canes. Other plastic distortions when, for example, tapers are drawn, cause gross geometrical distortions of an image transmitted through the fiber-optic part. Careful specification of limits to all these defects and distortions are needed for good

parts. Moreover, since the level of defects and distortions varies from one production run to another, careful monitoring of the delivered product is absolutely necessary to determine if the part is acceptable.

Actinide contamination refers to the inclusion of radioactive elements in the glass formulation. Most fiber-optic glass formulations contain rare earths and most rare earth oxide feed stocks are naturally contaminated with actinides, such as thorium.[105,106] Another source of actinide contamination is the polishing of parts with actinide-contaminated rouges, such as cerium rouges. Fiber optics in x-ray detectors are usually butted against CCDs or overlaid with phosphors, both of which are very sensitive to excitation by radioactive emissions stemming from decay of the actinides and their daughters. This results in bright spots, or so-called ''zingers,'' which accumulate in the detector images in proportion to the length of the exposure. The level of contamination may be very small in absolute terms (<1 ppm), but this still results in a significant cumulative signal in long integrations. X rays resulting from stopped radioactivity in the bulk of the fiber optics may also excite the phosphor or the CCD. The end result is that zingers are typically distributed in intensity from very bright to vanishingly dim and can be numerous. Some ''zinger'' removal is possible via digital manipulation of the x-ray image (see Sec. IV F), but this is troublesome. The best solution, of course, is to avoid the use of actinide contaminated fiber optics. In our experience, there is significant batch-to-batch variation in the level of actinide contamination in fiber optics from most vendors. This is really inexcusable, since the cause of the problem is understood. The best advice is to set a specification on the part and test the result to see if it is acceptable. Hopefully, fiber-optic vendors will eventually respond to customer demands for actinide-free parts.

One could potentially identify the sources of actinide contamination by examining decay spectra using various energy-resolving detectors. These detectors have very different responses to alpha, beta, and gamma decays, and it is not always possible to relate these specific activities to the problem that they will introduce in a detector. A simpler measurement that has direct bearing on detector performance is made by placing the fiber optic in direct contact with a phosphor on transparent mylar optically greased to the surface of a 2 in. photomultiplier tube. A very radioactive sample would still only result in a count rate of say 1 Bq for a 2-in.-diam active area. More typically, one observes count rates from several per minute to several per hour. With these count rates, we have found it practical to simply record tube current on a chart recorder and manually count events over a specified period of time.

2. Characterization of fiber optics. Several simple tests can be performed to assess the quality of a particular fiber optic before the unit is affixed to the CCD in the detector. Gross defects are easily seen by casual inspection. More subtle performance characteristics should be examined quantitatively.

Inspection of a large fiber optic for shear dislocations can be facilitated with the use of a pair of crossed Ronchi rulings.[101] The parallel lines in the rulings will normally create a regular Moiré pattern. When a fiber-optic part is placed between the rulings and one of the rulings is rotated to spread the Moiré fringes to infinity, distortions become quite evident. Even small shears will be shown as discontinuities in the Moiré pattern. Note that for fiber-optic tapers, the two rulings should have spacings in the same ratio as the taper to provide best results.

Light transmission will depend on physical parameters of the glass, such as the core/clad ratio, numerical aperture, and the taper ratio, as well as the particular fusing conditions used in making the fiber-optic bundle. Transmission will also depend on the angular distribution of the incident light as well as its wavelength. Light from a phosphor emanates with a Lambertian distribution. We have found good comparisons between various fiber-optic samples can be made using a standard light box with fluorescent tubes and a diffusing plate, such as opal glass. A photodiode is used to measure the light/unit area at the surface of the light box, and then again at the end of the fiber optic. Adjustment is made for the demagnification ratio by multiplying by a factor of $1/M^2$. Transmission is measured at several positions as transmission is usually expected to vary from center to edge. One should consider the changes in magnification that often occur from center to edge in this measurement as well. It should be noted that this measurement is affected by the quality of the EMA absorbers. For example, a fiber optic with no EMA will transmit much more light, but much of this light is scattered incoherently and only adds to the background noise and reduction in resolution.

Since a fiber optic is designed to transmit light along a fiber, as opposed to between fibers, a rough qualitative test of resolution (and the effectiveness of the EMA fibers) is to shine a strong light into the side of the fiber optic and look for light coming out the ends. Poor resolution bundles will easily show light up to 1 cm or more from the edge.

More quantitative testing can be made by shadowing a flood illumination with a knife edge mask and measuring the light intensity scattered into the region shadowed by the knife. Detector parameters are sensitive to light scattered at the 10^{-4} level or lower and as such, this test should be able to measure over this dynamic range. Measuring directly the light level in the unshadowed portion concurrently with the scattered signal is difficult. One can, however, attenuate the unshadowed portion at the fiber-optic output with a neutral density filter of a given value (see Fig. 12). Overlap of the neutral density filter onto the output of shadowed region is inevitable, but it becomes desirable in this case, since one can adjust the overlap region such that the intensity of the flood region can match the intensity just beyond the overlap region quite accurately with visual comparison alone. One then measures the distance the filter extends into the shadowed region. Measurements are usually taken for filters with neutral density values of 1.0 to 4.0.

The spread of light in the fiber optic depends critically on the angular distribution of the incident light, as well as its wavelength. Typically, light impinging at normal incidence spreads very little. We have also observed much more light spreading in the red wavelengths as compared to the blue or green, especially for some types of EMA. These factors

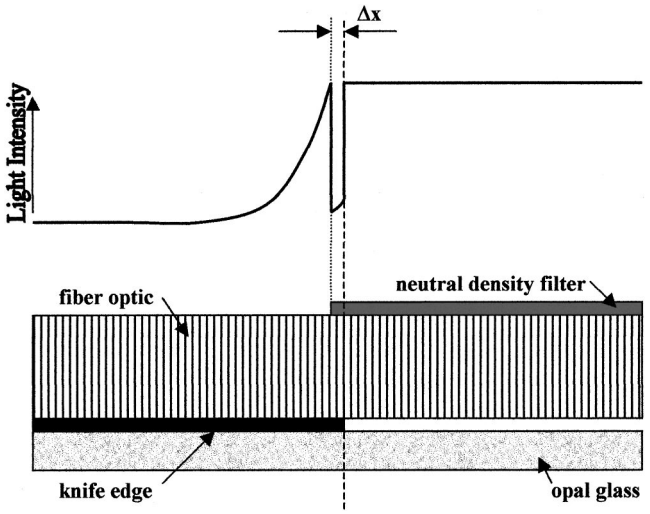

FIG. 12. Measurement of light spread in fiber optics. Here a fiber optic with a knife edge mask is illuminated from below using a source with diverging light such as an opal glass diffuser. A neutral density filter (O.D. 1.0 to 4.0) covering the illuminated portion of the fiber optic compresses the dynamic range required in the measurement system. The filter also provides a calibrated reference for the scattered light intensity in the unilluminated portion of the fiber optic. One can visually adjust the overlap of the filter (Δx) until the scattered intensity matches that transmitted through the filter. Measurements can then be repeated for various filter densities.

should obviously be considered when making tests for a given detector. Semiquantitative comparisons between fiber optics can be made if one uses a consistent light source. For thin fiber-optic blanks, we have found it convenient to make measurements on a microscope using the microscopes condensing illuminator and 100× magnification with eyepiece reticle. The knife edge consists of a piece of black vinyl electrical tape[107] affixed to one side. For large fiber-optic tapers, measurements can be made on a light box with most of the area masked off. Again, the edge is formed with black tape, and the source is the opal glass diffuser of the light box, against which the face of the taper is placed. Measurements can be made with a hand held magnifier with a reticle.

3. Coupling to fiber optics. Reliable, mechanically stable couplings between fiber optics and the CCD are necessary for a robust, stable detector system. The simplest solution, butting the fiber optic next to the CCD, suffers from a lower coupling efficiency and reduced resolution owing to the larger mismatch in the index of refraction between the fiber optic, intervening air, and the CCD.

Optical epoxies and clear silicone rubbers are possibilities for coupling, but these bonds must be able to withstand stresses of repeated thermal cycling between room temperature and a typical operation point of -20 to $-60\,^{\circ}\mathrm{C}$ or below. Not only must the bonding material be designed for these low temperatures, but the fiber-optic glass, the CCD and its mounting carrier should be matched as closely as possible in their thermal coefficients of expansion. We have had good success with two-part silicone coupling gels.[108] Needless to say, CCDs with small areas are much easier to bond reliably than larger ones since the stress from edge to edge is much less for the same temperature change.

Reliable joints require uniform, clean surfaces. Some generations of CCD chips have been notorious for their lack of flatness ($>20\ \mu$m). Good couplings in this case require the back end of the taper be ground and polished to match this shape.

An alternative to using a hard bond is to use a fluid filler such as an optical coupling oil (e.g., ''laser liquid,'' Cargille Laboratories, Inc., Cedar Grove, NJ 07009). Again, this material should remain fluid at the operation temperature. Additionally, a reliable means for containing the fluid long term is necessary, realizing the volume of the oil changes quite substantially between room temperature and the operating temperature. Additionally, an external mechanical coupling is required to keep the taper and CCD aligned. Movements of less than a pixel can be quite evident. In addition, if the gap between taper and CCD changes with time, the pattern of interference fringes between the two surfaces can change, necessitating frequent recalibrations for detector sensitivity. Advantages of this technique are that it allows the use of fiber optic glass which has a larger thermal mismatch to the CCD and the ability to bond larger area CCDs.

Bonding techniques for one CCD/fiber optic combination might not be appropriate for other systems. For example, back-illuminated CCDs are typically coated with an antireflection (AR) coating. A bond then has the potential to fail between the AR coating and the CCD when the thermal stress is applied.

D. Image intensifiers

1. When is intensification needed?

Image intensifiers are used to introduce gain between the x-ray converter and successive parts of the detector. In an intensifier, light falls on a photocathode that emits photoelectrons. The electrons are accelerated across a large voltage, say 10 keV, and impact, typically, into a phosphor. Since each electron now has 10 keV of energy, it results in the emission of many optical photons from the phosphor, i.e., produces optical gain.

Although intensifiers are expensive and delicate and, thus, to be avoided whenever possible, there are situations where they are invaluable. A simple example, along the lines of Eq. (2.16) and the discussion of Sec. II C 3, shows that intensification may be needed when it is necessary to efficiently couple a large area phosphor to a much smaller area optical sensor. It was desired to couple a phosphor on a demountable fiber optic plate to a CCD that had a permanently mounted 0.5 cm fiber optic faceplate.[109] A particularly low distortion 5:1 fiber-optic taper was available. It had a measured efficiency of 2.5% to green light. The phosphor had a measured output from the fiber-optics faceplate of 200 photons for each 5.9 keV x ray. The 70% efficiency at each of the two fiber-optics interfaces (phosphor faceplate to taper and taper to CCD faceplate), resulted in a net of 2.5 photons/x ray incident on the CCD. Folding in a 30% CCD quantum yielded an average of 0.8 photons/x ray, which was unacceptably low.

An intensifier coupled to the phosphor faceplate was used to improve the statistics. It was a custom fabricated proximity focused tube with input and output fiber optic windows and a 10% photocathode efficiency and an optical

gain of 39. Thus each x ray produced $200\times0.7\times0.1=14$ photoelectrons in the intensifier and $200\times0.7\times39\times0.7\times0.025\times0.7\times0.3=20$ electrons in the CCD, well above the 11 electrons read noise of the CCD. Note, incidentally, that the alternative approach of putting a smaller, less expensive intensifier *after* the taper would have resulted in the same average signal per x ray but a much noisier detector because there would be a spot along the signal chain, namely at the intensifier photocathode, where the number of quanta would have been too small. Specifically, the average number of photoelectrons/x ray in the intensifier would have been $200\times0.7\times0.025\times0.7\times0.1=0.2$. It is necessary to make sure that the number of quanta everywhere along the signal chain is sufficiently large such that signal fluctuations do not result in lost ''counts.''

Our example shows that intensification may be beneficial if the detector has a large demagnification ratio. Other situations in which intensification is useful follow from consideration of the assumptions of the example. A noisy position sensor at the end of the signal chain (e.g., a video-rate CCD camera) can be compensated by adequate gain before the sensor. Finally, intensification is useful if the required signal from each x ray should be much larger than the noise. This is the case, for example, for astronomical x-ray imaging in which the x-ray flux is extremely small and the detection of every x ray is important. So intensification should be considered in situations involving large demagnification ratios, noisy position sensors, or the need for very high signal-to-noise ratios.

2. Types of intensifiers

Overviews of image intensifiers are given by Rose[110] and by Johnson and Owen.[111] Additional information may be obtained from the major manufacturers of image intensifiers, which includes most of the large companies that make photomultiplier tubes.[112] Because the photoelectrons emitted by the photocathode are emitted in random directions, some method must be used to focus the electron image onto the intensifier output screen. Four categories of intensifiers may be distinguished by the focusing method employed: the image can be proximity, electrostatically, or magnetically focused, or a microchannel plate may be used. The relevant principles of operation as applied to CCD x-ray detectors are given in the next few sections.

1. Proximity focused intensifiers. Proximity focusing simply means that the output screen is kept sufficiently close to the photocathode that the electrons have little opportunity to drift parallel to the photocathode surface before impacting the output screen. The primary disadvantage of this method is that limited accelerating potentials can be sustained over the short distance needed to maintain a high-resolution image, thereby limiting the overall gain which is achieved. Resolution can be traded for gain by lengthening the accelerating gap. An advantage of proximity focusing is that it introduces no geometrical distortion into the image. Proximity focused tubes are available with clear glass or fused fiber-optic input windows, the latter being necessary if an input phosphor image is to be efficiently fiber optically coupled to the photocathode, as is usually desired for sensitive x-ray detection. Optical gains of about 50 are readily obtained. As is the case with all types of intensifiers, cascaded stages may be used to achieve higher overall gains. An example of a CCD detector based on a proximity tube custom built for the application is an intensifier/fiber optic/CCD detector described by Tate *et al.*[109]

2. Electrostatically focused intensifiers. Electrostatically lensed tubes use electrostatic lens elements to focus the image. These tubes are also known as inverter tubes because each lens element inverts the image. Electrostatic focusing is the only practical method of making reducing intensifiers with very large input areas and is most commonly used for medical radiological imaging. Medical image tubes, modified for use with softer x rays by the installation of beryllium windows and thinner photocathodes, are the basis for a number of detectors.[113,114] Electrostatic lenses usually require curved photocathodes for good focusing. For small diameter tubes this is usually done by making the input window out of fused fiber optics with a sculpted, curved photocathode surface. The disadvantages of electrostatic tubes include geometric image distortion (especially of the pin-cushion type), the need for a curved input window in large area tubes, and sensitivity to stray magnetic fields.

3. Magnetically focused intensifiers. In a magnetically focused intensifier, an accelerating potential is imposed between parallel photocathode and output screens. Simultaneously, a uniform magnetic field B along the accelerating direction causes the photoelectrons to execute helical paths from the photocathode to the output screen. The angular frequency of rotation of all the photoelectrons is the cyclotron frequency eB/m_ec, which depends only on the magnetic field and fundamental constants (i.e., the mass m_e and charge e of the electron and the speed of light c). Therefore, after each orbital period the electrons refocus back to the original photocathode image. Since the speed profile of the electrons along the electric field direction is essentially the same for all photoelectrons, there exist a succession of planes in space, separated temporally by the cyclotron period, where the photoimage is refocused. It is only necessary to adjust the accelerating potential and the magnetic field so that one of these planes is coincident with the output screen.

Magnetically focused intensifiers are capable of very high resolution and, since the photocathode and output screens are well separated, can sustain high accelerating potentials of 10 kV or so. Four stage intensifiers with optical gains of several million are feasible. The disadvantages of magnetically focused tubes are cost, susceptibility to stray magnetic fields, and some slight geometric s distortion due to nonaxial components of magnetic field. The size of the input area is also limited by the need for a uniform magnetic field.

An example of a CCD detector based on a magnetically focused intensifier is the intensifier/lens/CCD detector of Tate *et al.*[109]

4. Microchannel plate intensifiers. Microchannel plate intensifiers maintain the image by confining the electron paths to parallel microchannels in a perforated glass plate a few millimeters thick.[115] The plate is made of a glass with a

resistivity of some gigaohms per millimeter so that a potential impressed upon the two faces of the plate divides uniformly along the length of the channels. Photoelectrons are proximity focused onto the microchannel plate and execute accelerating, arcing collision paths into the walls of the channels. Each impact produces secondary electrons, which accelerate, collide, and produce more secondaries, etc. The result is high electron multiplication. The electron shower emerging from the microchannel plate is then proximity focused onto the output screen. Gains of several million are readily achieved in multistage tubes, which are usually of the zig–zag or chevron arrangement. Microchannel plate intensifiers are very compact, have practically no geometric distortion, are relatively robust, and comparatively insensitive to stray magnetic fields. In consequence, they have displaced the other forms of intensification in many imaging applications. Microchannel plate intensifiers are used, for example, in most modern night vision goggles.

Unfortunately, microchannel plates do not match the quantitative performance of other types of image intensifiers. The secondary multiplication process is very noisy; at relatively low potential, the histogram of the multiplication factors for single electron events, the so-called pulse height distribution, is exponentially distributed. This may be remedied by raising the potential across the microchannel plate so that most events saturate the channel, that is to say, effectively discharges the channel. This puts a well-defined peak in the pulse height distribution, corresponding to a well-defined electron multiplication factor, but at a price: the channel is dead until it can be recharged, which, due to the high resistivity of the channel, typically takes several milliseconds. The result is a local count rate limitation on the intensifier. Microchannel plates also have stability problems. The gain of a channel decreases over its lifetime. The change of gain may be as large as a factor of 2 and is a function of the total charge that has gone down that particular channel. As a consequence, microchannel plates do not maintain a long-term gain calibration under use.

Rodricks *et al.*[116] describe a multimodule CCD detector incorporating microchannel plate intensifiers.

3. Intensifier output screens

The output screen of an intensifier need not be a phosphor. The electron image can directly bombard a position sensor, such as a CCD.[117] The disadvantages of not converting the image to an intermediate light image is a loss of modularity and, most importantly, the danger of electron radiation damage to the CCD. The advantages include elimination of intervening phosphors and optical couplings and very high gain with a single stage of intensification. In the silicon intensified target (SIT) vidicon tube a single stage intensifier directly bombards a vidicon target, which is adequately radiation hard for long life. Phosphor-SIT vidicons have been the basis for single-stage x-ray detectors.[118]

4. Intensifiers: General considerations and future devices

Many intensifiers contain phosphors on fiber-optic parts. Optical distortions and blemishes in the fiber optics and ''zingers'' due to actinide excitation of phosphors by the fiber optics (see Sec. II C 3 1) can compromise the intensifier. Another consideration is that intensifiers typically have windows whose internal surfaces are at potentials of many kV. There is always some leakage through the window, leading to charging of the external surface. This can be fatal to CCDs, which are extremely sensitive to electrostatic discharge. For this reason, all windows supporting high voltage in the vicinity of a CCD should have an external ground plane, for example, by a grounded, conductive, transparent coating of indium tin oxide. Note that this may place special requirements on the voltage competency of the optical windows of the intensifier. Fiber-optic windows, in particular, have to be rated for high voltage, lest they break down over time and develop luminescent fibers.

In general, image intensifiers are expensive and suffer from a number of other problems. Photocathodes share common features with photomultipliers in that they have low quantum efficiencies, are easily damaged by exposure to intense light, and exhibit fatigue. The deposition of low dark current photocathodes is an art form. The most efficient, and therefore, popular, image tube phosphors exhibit persistence, which may necessitate custom phosphor screens and compromised gains. Field emission, which causes persistent bright spots, can be a problem. Intensifiers are vacuum tubes and, therefore, are mechanically fragile. Internal parts are suspended in vacuum and may be susceptible to vibration, especially since high potential parts usually have tight tolerances on their mutual separation. Over time, image tubes tend to accumulate residual gas (e.g., He), which causes bright scintillations known as ion spots. Intensifiers require very stable high voltage power supplies for stable gains.

It must be noted that the introduction of low noise CCDs has considerably decreased the demand for image intensifiers, with the result that there are fewer manufacturers today than a few decades ago. The manufacture of high quality image intensifiers demands a considerable infrastructure and is well beyond the capabilities of small laboratory groups. Ultimately, the limited availability of image intensifiers is the most severe constraint to their continued use.

A device that may someday overcome many limitations of vacuum tube intensifiers is a two-dimensional variant of the solid-state photomultiplier. Solid-state multipliers are monolithic, thickly depleted reverse-biased semiconductor diodes which have sufficiently high internal fields to effect carrier avalanche and multiplication. Small, nonimaging variants are now commercially available as replacements for photomultiplier tubes. High spatial resolution two-dimensional arrays of such devices are, in principle, possible.

E. Position sensitive arrays

The last element in the signal chain of Fig. 1 is the sensor which position encodes the signal. The most important position sensors for x-ray detectors include

(1) vacuum tube TV cameras;
(2) CCDs; and
(3) diode arrays, CIDs (charge injection device), and complementary metal-oxide semiconductor (CMOS) imagers.

1. Vacuum tube TV cameras

Although vacuum tube TV cameras, most notably vidicons, have been almost completely supplanted by solid-state sensors, vidicon-based x-ray detectors were important for the development of area x-ray detector technology. The essential aspects of modern CCD detector technology—phosphors, intensifiers, fiber optics, coupling procedures—were first developed for vidicon-based sensors; as a consequence, knowledge of this literature is important. A personal review has been given by Gruner.[119]

The remaining parts of this section will focus on solid-state sensors, since these are the devices which will be used in practically all cases in the future.

2. CCDs

Charge-coupled devices (CCDs) have revolutionized imaging technology. Hall[120] and Janesick and Elliott[52] provide exceptionally lucid and recommended reviews of CCDs. Early books on CCDs include Sequin and Tompsett[121] and Howes and Morgan.[122] Principles of operation are summarized by Tredwell[123] and Holst.[124] Volume 26, Nos. 8–10 of *Optical Engineering* (1987) contains collections of articles on CCDs. The Society of Photo-Optical Instrumentation Engineers (SPIE) publishes excellent books and video tape courses on the use of CCDs.[125] Practical books on the assembly of CCD cameras have been written for the amateur astronomy community.[126,127] Comments here will be confined to an overview and details which especially pertain to the use of CCDs in x-ray detectors.

A modern CCD typically consists of a silicon chip monolithically fabricated into distinct columns by implanted potential barriers called channel stops [Fig. 13(a)]. The surface of the silicon is overlaid with an insulating silicon dioxide or silicon nitride layer and this, in turn, is overlaid with rows of conducting electrodes, called clocking gates, running perpendicular to the columns. It is primarily the external voltages impressed upon the gates that define the separation of the pixels down the columns. Photocharges generated in the depletion region buried in the chip accumulate in the potential wells [Fig. 13(b)]. By clocking these potentials in a periodic way [Fig. 13(c)], the accumulated charge packets are systematically shifted down the length of the columns while still maintaining the separation of adjacent packets in the column. Thus, the CCD consists of a series of parallel analog charge shift registers organized into columns. The columns terminate in an analog output shift register perpendicular to the columns, which, itself terminates in the input structure of an on-chip preamplifier (13d). Because the capacitance presented to the preamp is very small—arising from a single pixel of the final shift register—CCDs are capable of noise figures of astonishingly few electrons.

In normal operation, the gates are clocked to simultaneously shift all the packets of charge down the column one pixel toward the output shift register. The pixels of charge that were immediately adjacent to the output shift register are clocked into the buckets of the output shift register. The output shift register is then clocked to sequentially shift the charge packets one at a time onto the input structure of the on-chip preamp. Once all pixels in the horizontal shift register have been so processed, the columns are again shifted down to load the output shift register with the next row of pixel charges, and so on, until all the pixels in the CCD have been clocked into the preamp. The fact that the pixels have to be processed one at a time onto the preamp sets a serial bottleneck that limits the rate at which the chip can be read out. Some CCDs are segmented into halves or quadrants, each with its own preamp, to improve the readout time. Although pixels can be clocked out of CCDs at rates of tens of MHz, the noise rises with the readout rate. For most CCDs, optimum noise performance occurs for cooled, slow-scan rates below 50–500 kHz, depending on the CCD and the analog to digital conversion electronics. At slow-scan rates, modern scientific CCDs readily achieve noise figures of 10 electrons rms/pixel. Noise figures of 5 electrons rms are not uncommon.

Cooling the CCD is generally needed to reduce the dark current of thermally generated electron-hole pairs. Dark currents on the order of $10\,e^-$/pix/s are routine at $-40\,^\circ$C, with much of the dark current coming from the $Si–SiO_2$ interface. This may drop by an order of magnitude or more by the use of multipinned-phase (MPP) CCDs, in which dopants implanted under certain of the gates allow biasing of the gates so as to drastically reduce $Si–SiO_2$ dark current. The use of MPP chips is becoming the norm in x-ray detectors.

Modern CCDs are buried channel devices. The term ''buried channel'' refers to an arrangement of the potential wells so the charges collect in the bulk of the silicon, well below the insulating overlayer. Buried channel operation turned out to be pivotal toward realizing high performance CCDs, because it keeps the charges away from the inevitable interface traps at the semiconductor/insulator junction. By keeping the charges buried below this interface, charge lifetime could be made very long (hours) and the charges could be efficiently shuttled from one end of the CCD to the other with little loss.

The potential well which confines the charges to a pixel is itself a function of the accumulated charge and only so many charges will fit into a well before it spills over, or blooms, into the next pixel. Most CCDs used in x-ray detector work have full-well capacities in the range of a few hundred thousand electrons and some have capacities of almost half a million. In general, the larger the full-well the better for x-ray detector work. Some CCDs have antiblooming structures built in, but this is not the norm for scientific CCDs. Janesick and Elliott[52] describe how MPP CCDs can be clocked in a clever way during integration so as to eliminate blooming. Unfortunately, few CCD controllers take advantage of this capability.

Fill factor refers to the fraction of the imaging area of the CCD that is photoactive. Serially readout CCDs with

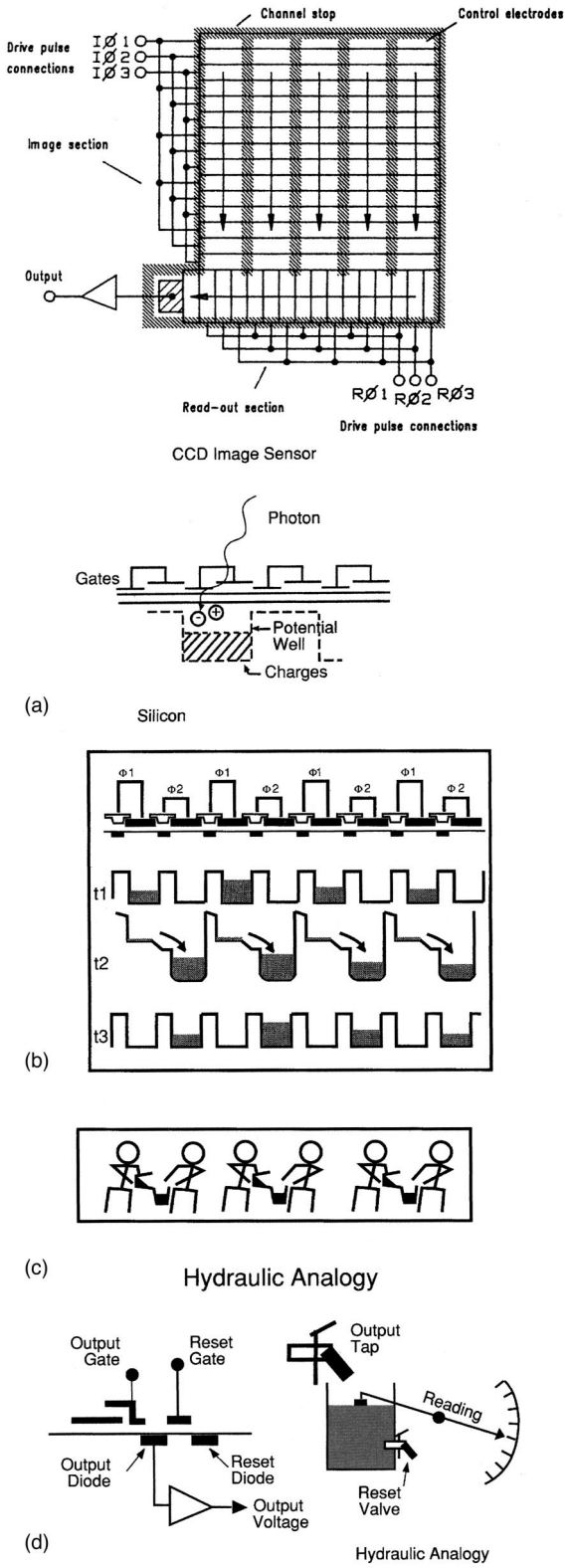

FIG. 13. (a) A CCD has columns defined by implanted channel stops and rows defined by overlaid electrodes. The crossings of the columns and the rows of electrodes define the pixels. The columns terminate in a output analog shift register. (b) Charges generated by light accumulate in the potential wells beneath each pixel. (c) The charges may be ''walked'' down the columns by an appropriate sequence of voltages clocked onto the electrodes. In a hydraulic analogy, the charges pass in bucket-brigade fashion down the column. The charges are transferred onto the output shift register and shifted onto the output gate of an on-chip preamp. Again, in a hydraulic analogy, the output *o* the preamp is proportional to the charge shifted onto the output gate. (a) is from (Ref. 207); and (b)–(d) are from (Ref. 208).

100% fill factor are most commonly used for x-ray detector work. These CCDs have the disadvantage that the imaging structure is also the readout structure, so image signal which arrives while the CCD is being read out winds up smeared over the shifting image already accumulated. Thus, it is usually necessary to stop the x-ray signal during read out, thereby imposing a duty cycle. For slow-scan operation at synchrotron sources, the time spent reading out the CCD may exceed the exposure time. Alternatively, interline or frame-transfer CCDs may be used. Interline transfer CCDs have a photoinsensitive shift register next to each column. The image to be read out is very rapidly (microseconds) transferred to the adjacent shift registers and the photopixels are then free to continue image accumulation while the shift registers are being clocked out. Interline transfer CCDs typically have less than unity fill factors due to the area taken up by the shift registers. In frame-transfer CCDs half of the length of the columns are covered and can be clocked independently of the uncovered half. These CCDs take advantage of the fact that the columns can be clocked down very quickly (microseconds) without compromising performance, i.e., the bottleneck starts at the preamp. So the image accumulated in the uncovered half of the columns is very rapidly clocked into the covered half, i.e., the frame is transferred. Then the transferred frame is slowly read out while the uncovered half integrates the next exposure. Although the uncovered half has 100% fill factor, the CCD must be twice as large to accommodate the storage frame.

CCDs are available in either front- or back-side illuminated versions. In front-side illuminated chips, the light passes through the polysilicon gates into the photosensitive bulk of the chip. Silicon is not very transparent toward the blue, which limits the blue sensitivity, typically to $<30\%$ at 550 nm and $<10\%$ at 450 nm. Alternatively, the CCD substrate may be thinned to about 10 μm and illuminated from the back, thereby limiting the path length of light through photoinsensitive absorbing material before entering the photoactive depleted region. In combination with antireflection coatings, this can improve the spectral response below 550 nm by factors of 2–3. The process of thinning a large area chip to 10 μm entails extra processing and inevitable loss of chips and, consequently, back-side-illuminated devices are very expensive. Moreover, since the demand for back-side-illuminated CCDs is low, there is limited availability of these CCDs. Recently, Kodak has introduced a series of CCDs in which the electrodes consist of transparent indium tin oxide, thereby enhancing blue sensitivity.[53]

CCDs are directly responsive to x rays, as well as to light. Their use as direct conversion x-ray detectors is limited both by stopping power and radiation damage concerns. The depletion regions of most commercially available CCDs are only a few microns thick, thereby presenting a small active cross section for hard x rays. The radiation damage problem is also a concern, since the cost of large CCDs is so high. Although the mechanisms of radiation damage are complex, the most severe problem at typical crystallographic x-ray energies is charging of the oxide. Hole mobility in SiO_2 is very small, whereas electrons leak through relatively quickly. This results in the build up of a positive space charge in the oxide

that changes the potential felt in the silicon underneath. Since the effect is dependent on the local exposure history, it cannot be trivially compensated for by changing the gate potentials. CCDs made of high resistivity material, which can be deeply depleted, have been built.[128–133] Some of these devices were designed to be resistant to radiation damage. A number of authors have evaluated deep-depletion CCDs for x-ray applications.[7,134–139]

CCD fabrication is a very demanding technology with the result that even good processes have low yields of blemish-free devices. As a consequence, top grade large area CCDs are very expensive—prices in excess of $10 000 are not uncommon and, in some cases, prices approach $100 000. CCDs are usually graded according to the density of point and column defects, with lower grade devices commanding considerably less money. It is important to realize that lower grade devices may very well still have $>99\%$ unblemished area and exhibit the same noise performance as top grade devices.

The performance of a CCD is also limited by the electronics of the CCD controller. A CCD with a full well of 4×10^5 electrons and a noise of 5 electrons has an intrinsic signal-to-noise ratio of 80 000. The off-chip analog signal chain must be designed with great care to realize this performance. CCDs also have many different modes of operation, involving various speeds and sequences of clocking the gates, ranges of clocking voltages, etc., and a controller capable of taking full advantage of this flexibility necessarily has some relatively unused features and high cost.

The CCD end of a CCD detector generally has three parts: The detector body, which includes the cooled CCD head, i.e., the CCD socket, cooling arrangement and electronics immediately adjacent to the chip; the CCD; and a remote CCD controller and associated computer. Typically, the CCD is fabricated by one vendor, the controller by another, and the detector body is often built by a third vendor. The market for scientific CCD controllers is dominated by a small number of vendors and the quality of the products ranges widely. Important considerations in selecting a controller include robustness of the hardware, software, quality of the analog to digital signal chain, flexibility and ease of adjusting the clocking patterns, the difficulty of changing from one CCD to another, cooling capabilities and, if one is building ones own detector body, the assistance the vendor provides in designing the CCD head. The last point is crucial, since proper design of a CCD head is nontrivial.

There are significant advantages of efficiency, radiation damage protection, and stability of calibrations afforded by bonding CCDs directly to fiber optic bundles.

3. Diode arrays, CIDs, and CMOS imagers

We close this section with mention of diode arrays. A diode array is simply an array of reverse-biased diodes that are addressed in $x-y$ fashion. The simplest incarnation is an array of diodes that is addressed by an array of horizontal (x direction) polysilicon electrodes lines on one side of a fully depleted silicon wafer and an array of vertical (y direction) electrode lines on the other side of the wafer. Any pixel may be addressed by selecting the x and y lines which cross at the pixel. Diode array detectors are distinguished by the way in which the signal is read out. An early competitor to the CCD was the CID.[140–143] Whereas charge is shifted out in a CCD, it is the $x-y$ matrix addressed in the CID though a clever set of electrodes onto an on-chip amplifier. Because the on-chip preamp now sees the full capacitance of the electrodes to the pixel, the noise is much higher than with CCDs. On the other hand, the image is fully addressable, so a small desired part (e.g., the expected positions of an x-ray spot) can be read out. Finally, the CID can be nondestructively read out by a clever procedure that does not destroy the accumulating image. By repeatedly nondestructively reading out the same image and averaging, the noise can start to approach CCD values. The practicality of this approach for full-frame readouts is limited, since the noise falls as the square root of the number of frames averaged together, so hundreds of reads may be required for each low noise frame. Examples of x-ray detector applications of CIDs are given by Hanley *et al.*[144]

The CMOS imager is a modern competitor to the CCD.[145–149] Whereas CCDs require specialized silicon foundries, CMOS imagers are made using normal CMOS fabrication techniques, thereby realizing important advantages in cost. A CMOS imager consists of a diode array in which CMOS fabrication is used to make a diode array with active switching transistors in each pixel. Although CMOS imagers have not achieved the low noise of the best scientific CCDs, their cost and flexibility of architecture make them a potent future competitor to the CCD for many applications.

III. REALIZED DETECTORS

It is clear from the preceding sections, that many configurations of detector components have been constructed. The literature on CCD detectors is too large to list every detector that has been reported; therefore, with a few exceptions, we reference a large sampling of CCD detectors that were designed for x-ray analytical purposes. Somewhat arbitrarily, we divide realized CCD detectors as to whether they contain image intensifiers,[113,114,116,150–159] use phosphors without image intensification,[5,97,98,100,160–174] or ones in which the x rays are captured by the CCD itself.[7,129,130,135,137,139,175–179] Some overviews of CCD detectors are included in Refs. 3, 180–183.

The decisions that dictate the use of a given configuration depend crucially on the details of the application, and the cost and availability of components. However, a general rule of thumb applicable to most applications is clear: the smaller the number of components in the optical relay (Fig. 1), the better the quantitative performance and long-term ability to maintain the calibration required for quantitative accuracy. Thus, simple combinations of phosphors coupled to CCDs are generally to be preferred over intensified detectors. Direct conversion of x-ray within radiation-hardened deep-depletion CCDs is even better, assuming that the CCDs can be obtained to cover the required area at an acceptable cost and with an acceptable lifetime.

IV. DETECTOR CHARACTERIZATION AND CALIBRATION

The quantitative usefulness of any detector depends on the degree to which it has been characterized and calibrated. Detector characterization and calibration have been discussed by many authors.[76,184–191] In this section we summarize the factors most relevant to CCD detectors (see, especially, Barna *et al.*[76]). These include

(1) spatial resolution;
(2) intensity (flat-field) calibrations;
(3) energy and angular calibrations;
(4) geometric distortions;
(5) background subtractions;
(6) detective quantum efficiency; and
(7) zingers and other considerations.

A. Spatial resolution

The measurement of the spatial resolution of a CCD detector was discussed in Sec. II B 1 8 on phosphor resolution. The assumptions which were made about the PSF, namely, that it is cylindrically symmetric, independent of intensity, and translationally invariant, are reasonable approximations for most phosphor screens. The ranges over which these are good approximations are likely to be more limited for the detector as a whole, especially at the extremes, e.g., near the edges of the detector or near saturation. In fact, breakdown of these approximations are often used as practical indicators of the usable ranges of values of the detector.

B. Intensity (flat-field) corrections

Many factors contribute to variation in sensitivity across the face of a typical CCD detector, including nonuniformities in the phosphor, the optical couplings, the transmission of the fiber optics, and the response of the CCD pixels. These nonuniformities are almost always sufficiently large as to require calibration for accurate quantitative work. Calibration involves exposing the detector to a known signal and mapping out the pixel-by-pixel response of the detector. This procedure is complicated by many factors:

(i) It is difficult to produce a uniform, known x-ray signal broad enough (i.e., a uniform flood field) to cover the face of large area detectors. Procedures for doing this are discussed by Moy[190] and by Barna *et al.*[76] The alternative, namely to scan a known, small area signal across the detector, can be very tedious. A tremendous number of x rays need to be accumulated for good statistics. So, e.g., from Poisson statistics alone, to flat-field correct a 1000×1000 pixel detector to an accuracy of 0.5% requires at least 4×10^4 x rays/pixel or 4×10^{10} x rays.

(ii) The PSF complicates the use of flood fields because the signal recorded at each pixel involves contributions from the signal, referred to the input face, of neighboring pixels. Ideally, one wishes to deconvolute the PSF out of the recorded image, but in practice, the PSF is rarely sufficiently uniform to allow this. The alternative, namely to scan the face of the detector with a signal that is small compared to the FWHM of the PSF is tedious to the point of impracticality. For these reasons the usual procedure is to use a flood field and accept the resultant limitations on accuracy. This consideration highlights the importance of a narrow PSF in order to minimize these limitations and allow more accurate flat-field calibrations.

(iii) Subpixel granularity limits the uniformity of response. Granularity arises from the microstructure of the phosphor screen, fiber optics, and CCD, as well as from dust and imperfections in the optical couplings. Granularity may be observed by scanning a stable micro-x-ray beam (i.e., small compared to a pixel) across a pixel in subpixel steps. One observes reproducible variations in the integrated response. The practical effect of granularity and the width of the PSF is to limit the accuracy with which small-area signals may be calibrated.

(iv) Geometric distortions, such as those typically encountered with fiber optic tapers and electrostatically focused intensifiers, may not be area preserving (see Sec. IV C). This means that the factor that maps small unit areas on the detector input onto the detector output varies with position on the detector face. The result is that the flat-field calibration must account for the way in which the geometric distortion compresses and expands a signal of a given magnitude and size over the output area. This illustrates the interaction between geometric and flat-field corrections. One way to deal with this is to first geometric distortion correct the images used to determine the flat-field correction. This is discussed in Barna *et al.*[76]

The practical effects of these complications are that it is often straightforward to flat-field correct a CCD detector for signals several pixels across to an accuracy of a few per cent of the intensity. It is much more difficult to flat-field correct to 0.5%. The difficulty of flat-field correction rises as the signal shrinks in size. Signals on the order of a pixel width across can rarely be corrected to better than a percent or so. Because of these complications, the flat-field corrections claimed in the literature for many (if not most) CCD detectors are optimistic. In this regard, note that the most serious limitations arise from the phosphor, fiber optics, and optical couplings. Further, the range in silicon of electron-hole production from a typical 5–10 keV x ray is only about a micron, so direct conversion CCDs have a near ideal single pixel PSF. It is likely that direct conversion CCDs can be calibrated to greater accuracy than phosphor-based detectors.

C. Energy and angular corrections

The amount of signal from a CCD detector may vary in a complicated way with the x-ray energy and angle of incidence. This is especially true for detectors with settled phosphor powder screens, which represent a majority of commercially available CCD detectors.[47] This is the result of two competing processes: first, the absorption efficiency is greater for obliquely incident x rays because of the longer path length through the phosphor. Second, the luminescence

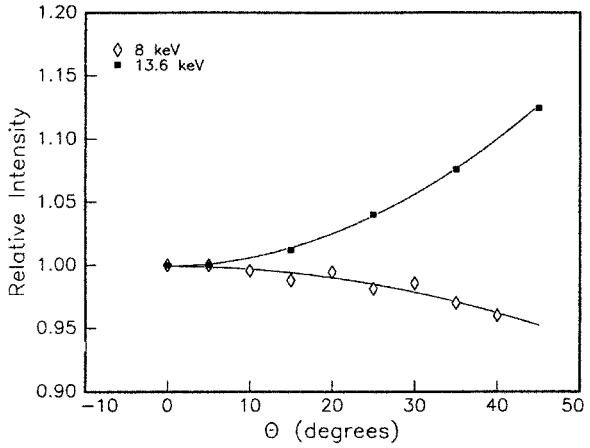

FIG. 14. The luminescent response of a settled powder phosphor screen vs angle for two different x-ray energies. At high x-ray energies, the angular effects are dominated by stopping power. At lower energies, the response is dominated by light loss. From Gruner *et al.* (Ref. 47).

is attenuated as it travels through the phosphor, so x rays that are stopped nearer to the incident surface yield less light. Thus, x rays that are obliquely incident tend to be stopped nearer to the incident surface and yield less light than normally incident x rays of the same energy. At low x-ray energies, most of the x rays are stopped in the phosphor. But at high x-ray energies a significant fraction of the normally incident x rays are not stopped in the phosphor at all, in which case, the increased absorption with angle results in more stopped x rays and more light. At intermediate x-ray energies, there will be angles where the two effects cancel. The angle effect is not negligible and can easily change the recorded luminescence per x ray by 10% or more (Fig. 14).

The response of the detector as a function of energy and incident angle is measured by exposing the detector to a monochromatic beam of x rays of the appropriate energy and angle. A monochromator arrangement working off the bremstrahlung background of a laboratory x-ray tube is suitable for making the measurements. It is of course necessary to collimate the beam to accurately define the angle and to use an scintillator/phototube combination to determine the number of x rays/s in the beam at each angle and energy. Barna *et al.*[76] found that the measured response is well fit by a two-dimensional surface given by

$$I(\theta,E)=I(0)+a(E)\theta^2, \tag{4.1}$$

where θ is the angle of incidence with respect to the screen normal, $I(0)$ is the response at normal incidence for a given x-ray energy, and a is an empirically determined function of energy. The angle/energy effect is smooth and slowly varying, so a sparse set of measurements at perhaps four energies for each of four angles is often sufficient to map out the full response. A least squares fit to the resultant two-dimensional surface results in a small number of coefficients that provide a compact way to compute the needed correction over the range of incident angles and x-ray energies.

D. Geometric distortions

Geometric distortions of the recorded image result primarily from image intensifiers and from the optical couplings in the system. Geometric distortions may be area preserving (affine) or nonarea preserving (rubber-sheet) transformations. Insofar as the distortions are smooth and slowly varying, they can be calibrated out. The most common calibration procedure is to use a shadow mask with a known, fine pitch of holes on a regular lattice. It is clearly necessary for the mask to be accurately made with an array pitch that is small compared to the scale of the distortion. Barna *et al.*[76] uses a lithographically fabricated array of 75-μm-diam holes on a 1 mm pitch in a 50-μm-thick tungsten mask. It is also important to place the mask as close as possible to the detector face and to illuminate it with an x-ray source sufficiently far away to avoid parallax effects. The x and y centroids of the spots in the recorded image are fitted with cubic polynomials, from which one computes an interpolated transformation from the incident to the recorded image.

A check on the distortion correction procedure is to distortion-correct an image of the shadow mask after a random rotation and displacement. The resultant centroids of the corrected image should be nearly identical with a perfect lattice to better than a small fraction of a pixel. The procedure used by Barna *et al.*[76] resulted in less than 0.25 pixel deviation from a perfect lattice for all centroids on a 1024 $\times$1024 pixel CCD detector with 50 μm pixels.

As noted in the discussion on fiber optics (Secs. II C 3), fused fiber-optic bundles are subject to discontinuities, called shear distortions. These cannot be accounted for with anything less than a pixel-by-pixel calibration procedure, which is usually quite impractical. A better approach is to use fiber optics with a tight specification on shears.

Fiber optic tapers usually introduce rubber sheet distortions that necessitate coupled flat-field and geometric distortion corrections. See the discussion on the flat-field correction, above, and Barna *et al.*[76]

E. Background subtraction

CCD detectors generally have two sources of zero x-ray dose instrumental background which need to be subtracted to obtain the true intensity of recorded images. The instrumental background arises from (a) CCD dark-current and (b) an intentional offset (pedestal) voltage of the electronics to avoid poor electronic behavior at near-zero voltage. At low temperatures, and especially for MPP CCDs, the dark current may be sufficiently small to allow integrations many hours long. Typical values are $1.0-0.01\,e^-$/s/pix in the range of -20 to $-50\,^\circ$C. The rate of dark current accumulation varies from pixel to pixel, so the zero-dose background I may be characterized as

$$I(x,y,t)=I_0(x,y)+a(x,y)t, \tag{4.2}$$

where $I_0(x,y)$ is the zero-dose, zero-time map and $a(x,y)$ is the pixel-by-pixel rate of accumulation. These parameters may be empirically determined and stored. However, it is usually safer to simply acquire occasional zero-dose expo-

sures of the required length of time to use as a background subtraction. Note that the dark current normally decreases by a factor of 2 for about every additional 7 °C drop in temperature, so temperature stability is important for stable backgrounds. It is good practice to stabilize the CCD temperature to better than 0.1 °C.

F. Detective quantum efficiency (DQE)

The DQE[72,184] is a measure of the overall system efficiency. It is defined as

$$\mathrm{DQE}=\left(\frac{S_o}{\sigma_o}\right)^2 \Big/ \left(\frac{S_i}{\sigma_i}\right)^2=(\mathrm{SNR}_o)^2/(\mathrm{SNR}_i)^2, \tag{4.3}$$

where, S=signal, σ=noise, and the subscripts o and i refer to input and output of the detector, respectively. All input signals have noise, e.g., for a Poisson input of a mean of N x rays, the $(\mathrm{SNR}_i)=N/\sqrt{N}=\sqrt{N}$. Hence, the DQE measures the additional noise imparted by the detection process. If the DQE=1, then no additional noise is added and the $\mathrm{SNR}_o=\mathrm{SNR}_i$, i.e, the detector, is an ideally noiseless detector. Note that a signal recorded with a noiseless detector is not necessarily noiseless because the signal itself has noise. Noisy detectors have $\mathrm{DQE}\ll 1$.

To model the DQE, one writes down expressions for the noise and signal of each element in the serial signal relay (Fig. 1) and then combines all these into an equation specifying how the detected signal and cumulative noise propagates through the detector.[2,101,175,184,186,192–196] Modeling the DQE can aid in detector design by identifying detector components which dominate the overall noise behavior. The DQE of the system can never exceed the DQE of the noisiest link in the serial signal relay.

As an example, consider the primary phosphor in a phosphor-based CCD imager. If the phosphor stops a fraction, a, of the incident x rays, then the DQE of the phosphor is given by

$$\mathrm{DQE}=a/(1+g^{-1}), \tag{4.4}$$

where g is the mean number of visible photons/x-ray emitted by the phosphor. Since g is typically very large (several hundred), the DQE of the phosphor is dominated by the stopping power, which in turn becomes the upper limit of the system DQE. For many very low noise detectors, the stopping power of the phosphor is a good approximation to the DQE. This makes excellent intuitive sense: suppose the detector were truly ideal, except for the limited stopping power of the primary x-ray converter. Then, from the definition of the DQE [Eq. (4.3)], setting $\mathrm{DQE}=a$, and recognizing that for N incident photons obeying Poisson statistics, $(S_i/\sigma_i)^2=(N/\sqrt{N})^2=N$, we have $aN=(S_o/\sigma_o)^2$. In other words, the output signal has identical statistics to an input signal of aN x rays.

The DQE will be seen to be functionally dependent upon practically every aspect of the detector and the measurement, including, the area of the integrated signal, the detector dark current, and the rate of signal read out. Although the DQE is useful in the design process, detailed performance claims based on numerical evaluation of the DQE from a model are always suspect. The numbers that go into the model are rarely known to great accuracy. Further, the model assumes complete knowledge of all noise sources and signal behavior in a complicated piece of apparatus. Hence, the *actual* DQE should always be measured.

In principle, the DQE can be measured by taking a sequence of nominally identical x-ray exposures and computing the variance in the integrated intensity for various areas in the exposures.[72,184] An accurate measurement of the DQE requires attention to many details and, in our experience, is rarely done properly. Care must be taken to accurately account for signal-to-noise in the incident signal and for subtle interactions between the DQE and the way in which the measurement is taken. For example, failure to account for the effects of signal averaging due to the PSF have led to many overestimations of detector efficiency. A method which is particularly prone to this type of error is the computation of signal variance based on the integration of small subareas of a flood field.[47,76]

In general, the type of signal used to measure the DQE should be as similar as possible to the signals of the intended application. Thus, the signals used to characterize detectors intended for crystallography should ideally be spots similar in area to crystallographic spots. In order to accurately include noise arising from detector calibrations, images should be calibrated, just as real data would be, before computing variances. In order to more realistically account for the accuracy of calibrations, the detector should be displaced parallel to it's face between each measurement so that a given incident calibration spot falls on different parts of the detector face. A general consequence of all these factors is that the DQE of a CCD detector is larger for small integrated features than for larger features.[197] This is ultimately a consequence of the fact that granularity and signal spreading inherent in the detector PSF makes it very difficult to accurately determine the response of the detector to a signal smaller than a pixel, as discussed in the preceding section. The best, in principle, way to measure the detector DQE (and generate the calibrations) is to measure the detector response, point by point, for a signal which is small compared to the half width of the PSF. However, this approach is practically impossible for detectors with very large numbers of pixels.

G. Zingers and other considerations

As discussed in the section on fiber optics, CCD detector images are prone to an accumulation of occasional (few/frame/s) spurious spots, called zingers, which range in intensity from barely above background to very bright. Besides specifying CCD parts with low levels of actinide contamination, there is little one can do but to ignore or remove the zingers. Ignoring the zingers is typically done for short exposures with sparse data, such as with protein crystallographic images at a synchrotron source. Barna *et al.*[76] describe two methods for zinger removal. The first is based on simple cross comparison of two nominally identical images. Since the zingers are sparse and occur randomly, there is a very low probability that two zingers will occur at the same location in two images. The second method is based on the

fact that that the intensity associated with zingers falls outside of the Poisson statistics of the local x-ray intensity and, therefore, can be identified to an acceptable level of confidence. This second procedure can be used even with single images, as long as the x-ray image has no sharp, high-contrast features. This is useful, for example, for radiography and for diffuse x-ray scattering from liquids and gasses.

Other considerations concern the stability of calibrations. In the experience of the authors, calibration data for well-built fiber optically coupled phosphor-based CCD detectors are remarkably stable over time spans of many months. Even so, occasional calibration is required for the most accurate data. Other types of CCD detectors may need to be calibrated more frequently. Specifically, detectors containing air or vacuum optical paths need to be monitored because of the accumulation of dust or film on optical surfaces. This occurs even with hermetic sealing unless great precautions are taken to avoid materials which can outgas organic film-making substances. Detectors containing image intensifiers are particularly susceptible to drifts in high voltages and changes in ambient magnetic fields. Stray magnetic fields are sufficiently deleterious that it is sometimes necessary to encase the detector in magnetic shielding materials (e.g., mu-metal). Even then, routine stray magnetic fields can cause calibration drifts.

V. FUTURE DETECTORS

CCD detectors have had an enormous impact on many x-ray applications, such as protein crystallography. While the use of CCD detectors is certainly expected to continue to grow, emphasis within the detector development community is shifting towards other solid-state sensor architectures that promise considerably more power and flexibility. The components in most CCD detectors (e.g., fiber optics, image intensifiers, CCDs, etc.) have typically been developed for visible light applications and adapted to x-ray detector use. Deep-depletion CCDs are notable exceptions in that they utilize the integrated circuit (IC) technology infrastructure to fabricate custom radiation sensors. The IC infrastructure is powerful and increasingly accessible, making it attractive to consider alternative sensor architectures.

One of the most attractive alternative architectures is an array of directly radiation-detecting pixels, each with its own processing electronics. Several groups around the world are currently working on such ''pixel array detectors'' (PADs). Although many PAD variants are being explored, the most common theme is to assemble two-layer devices that are connected, pixel-by-pixel, via lithographically fabricated metal connecting ''bumps'' (bump-bonding). The x rays are stopped in a thickly depleted, high-resistivity semiconductor layer. The resultant charges are conveyed via the connecting bumps to the second layer, which is fabricated in CMOS. This architecture has many advantages: the radiation-detecting layer is a relatively simple matrix of diodes, which is relatively simple to fabricate and can be made out of non-standard semiconductors, such as high-resistivity silicon, germanium, or other high-stopping power materials. Thus, this layer can be tailored for x-ray detection. The CMOS layer is fabricated by standard, commercial silicon foundries using normal IC design rules. This allows much flexibility in the design of the functional electronics in each pixel. PADs can be analog, digital, or hybrid detectors. Although it is beyond the scope of this review to survey PAD technology, a few representative references illustrate the power of the approach.[198–206]

ACKNOWLEDGMENTS

The authors have had the pleasure of working with many students and colleagues on detector research. We wish to especially acknowledge those for whom detectors have been a primary effort: Sandor Barna, Alper Ercan, John Lowrance, Jim Milch, Matt Renzi, George Reynolds, Giuseppe Rossi, John Shepherd, Richard Templer, and Bob Wixted. We have also enjoyed detector support from the NSF, NIH, ONR, and, most especially, from the Office of Biological and Environmental Research of the Department of Energy (Grant No. DE-FG-0297ER62443), which has supported our detector research for many years.

[1] M. W. Tate, Adv. X-Ray Anal. **34**, 357 (1991).
[2] M. Stanton, W. C. Phillips, D. O'Mara, I. Naday, and E. Westbrook, Nucl. Instrum. Methods Phys. Res. A **325**, 558 (1993).
[3] N. M. Allinson, J. Synchrotron Radiat. **1**, 54 (1994).
[4] C. M. Castelli *et al.*, Nucl. Instrum. Methods Phys. Res. A **391**, 481 (1997).
[5] M. Suzuki, M. Yamamoto, T. Kumasaka, K. Sato, H. Toyokawa, I. F. Aries, P. A. Jerram, D. Gullick, and T. Ueki, J. Synchrotron Radiat. **6**, 6 (1999).
[6] W. C. Phillips, M. Stanton, A. Stewart, H. Qian, C. Ingersoll, and R. M. Sweet, J. Appl. Crystallogr. **33**, 243 (2000).
[7] F. Livet, F. Bley, J. Mainville, R. Caudron, S. G. J. Mochrie, E. Geissler, G. Dolino, D. Abernathy, G. Grubel, and M. Sutton, Nucl. Instrum. Methods Phys. Res. A **451**, 596 (2000).
[8] B. A. H. Kevles, *Naked to the Bone. Medical Imaging in the Twentieth Century* (Rutgers University Press, New Brunswick, NJ, 1997).
[9] E. Danielson, M. Devenney, D. M. Giaquinta, J. H. Golden, R. C. Haushalter, E. W. McFarland, D. M. Poojary, C. M. Reaves, W. H. Weinberg, and X. D. Wu, Science **279**, 837 (1998).
[10] J. Wang, Y. Yoo, C. Gao, I. Takeuchi, X. Sun, H. Chang, X.-D. Xiang, and P. G. Schultz, Science **279**, 1712 (1998).
[11] W. H. Green, K. P. Le, J. Gray, T. T. Au, and M. J. Sailor, Science **276**, 1826 (5320) (1997).
[12] G. Blasse and B. C. Grabmaier, *Luminescent Materials* (Springer, Berlin, 1994).
[13] G. F. J. Garlick, *Luminescent Materials* (Clarendon, Oxford, 1949).
[14] H. W. Leverenz, *An Introduction to Luminescence of Solids* (Dover, New York, 1968).
[15] D. Curie, *Luminescence in Crystals* (Wiley, London, 1963).
[16] J. B. Birks, *The Theory and Practice of Scintillation Counting* (MacMillan, New York, 1964).
[17] J. L. Ouweltjes, Mod. Materials **5**, 161 (1965).
[18] A. P. D'Silva and V. A. Fassel, *X-ray Excited Optical Luminescence of the Rare Earths*, Handbook on the Physics and Chemistry of Rare Earths (North-Holland, New York, 1979).
[19] G. Blasse, Prog. Solid State Chem. **18**, 79 (1988).
[20] G. Blasse, Chem. Mater. **1**, 294 (1989).
[21] G. Blasse, Adv. Inorg. Chem. **35**, 319 (1990).
[22] TEPAC, *Optical Characteristics of Cathode Ray Tubes*, Publication TEP116-B (Electronics Industries Association, Washington, D.C., 1987).
[23] Aktiengesellschaft Riedel-de Hahn, Wundtorfer Strasse 40, D-3016 Seelze 1, Germany; in the U.S., Hoechst-Celenase Corp., 5200 77 Center Drive, Charlotte, NC 28217.
[24] GTE-Osram, Hawes St., Totowa, PA 18848.
[25] Harshaw Bicron, 6801 Cochran Rd., Solon, OH 44139.
[26] Nichia America, 1006 New Holland Ave., Lancaster, PA 17601.

[27] G. F. J. Garlick, in *Handbook der Physik*, edited by S. Flugge (Springer, New York, 1958), Vol. XXVI, p. 1.
[28] S. E. Derenzo, W. W. Moses, J. L. Cahoon, R. C. C. Perera, and J. E. Litton, IEEE Trans. Nucl. Sci. **37**, 203 (1990).
[29] G. Blasse, IEEE Trans. Nucl. Sci. **38**, 30 (1991).
[30] A. D. Dinsmore, D. S. Hsu, H. F. Gray, S. B. Qadri, Y. Tian, and B. R. Ratna, Appl. Phys. Lett. **75**, 802 (1999).
[31] S. R. Jansen, J. M. Migchels, H. T. Hintzen, and R. Metselaar, J. Electrochem. Soc. **146**, 800 (1999).
[32] J. A. Shepherd, S. M. Gruner, M. W. Tate, and M. Tecotzky, Proc. SPIE **2519**, 24 (1995).
[33] J. A. Shepherd, S. M. Gruner, M. W. Tate, and M. Tecotzky, Opt. Eng. (Bellingham) **36**, 3212 (1997).
[34] X. D. Sun and X. D. Xiang, Appl. Phys. Lett. **72**, 525 (1998).
[35] S. Yang, C. Stoffers, F. Zhang, S. M. Jacobsen, B. K. Wagner, C. J. Summers, and N. Yocom, Appl. Phys. Lett. **72**, 158 (1998).
[36] H. Yamada, A. Suzuki, Y. Uchida, M. Yoshida, H. Yamamoto, and Y. Tsukuda, J. Electrochem. Soc. **136**, 2713 (1989).
[37] A. Koch, C. Raven, P. Spanne, and A. Snigirev, J. Opt. Soc. Am. A **15**, 1940 (1998).
[38] A. L. N. Stevels and A. D. M. Schrama-de Pauw, Philips Res. Rep. **29**, 340 (1973).
[39] H. Washida and T. Sonoda, Adv. Electron. Electron Phys. **52**, 201 (1979).
[40] V. V. Nagarkar, T. K. Gupta, S. R. Miller, Y. Klugerman, M. R. Squillante, and G. Entine, IEEE Trans. Nucl. Sci. **45**, 492 (1998).
[41] H. S. Cho, W. S. Hong, V. Perez-Mendez, J. Kadyk, N. Palaio, and J. Vujic, IEEE Trans. Nucl. Sci. **45**, 275 (1998).
[42] H. W. Deckman, J. H. Dunsmuir, and S. M. Gruner, J. Vac. Sci. Technol. B **7**, 1832 (1990).
[43] C. G. A. Hill, P. E. Lovering, and A. L. G. Rees, Trans. Faraday Soc. **43**, 407 (1947).
[44] M. Sadowsky, J. Electrochem. Soc. **95**, 112 (1949).
[45] S. Pakswer and P. Intiso, J. Electrochem. Soc. **99**, 164 (1952).
[46] N. A. Diakides, Proc. SPIE **42**, 82 (1973).
[47] S. M. Gruner, S. L. Barna, M. E. Wall, M. W. Tate, and E. F. Eikenberry, Proc. SPIE **2009**, 98 (1993).
[48] M. J. Shane, J. B. Talbot, R. D. Schreiber, C. L. Ross, E. Sluzky, and K. R. Hesse, J. Colloid Interface Sci. **165**, 325 (1994).
[49] M. J. Shane, J. B. Talbot, B. G. Kinney, E. Sluzky, and K. R. Hesse, J. Colloid Interface Sci. **165**, 334 (1994).
[50] Fres-co System USA, Inc., 3005 State Rd., Telford, PA 18989.
[51] S. J. Henderson, J. Appl. Crystallogr. **28**, 820 (1995).
[52] J. Janesick and T. Elliott, in *Astronomical CCD Observing and Reduction Techniques*, edited by S. B. Howell (Astronomical Society of the Pacific, San Francisco, CA, 1992), pp. 1–67.
[53] Kodak Blue Plus CCD series, www.kodak.com/go/ccd
[54] C. I. Coleman, Adv. Electron. Electron Phys. **64B**, 649 (1985).
[55] D. J. Robbins, J. Electrochem. Soc. **127**, 2694 (1980).
[56] A. Bril, in *Luminescence of Organic and Inorganic Materials*, edited by H. P. Kallmann and G. M. Spruch (Wiley, New York, 1962).
[57] A. Bril and A. de Poorter, J. Electrochem. Soc. **122**, 1086 (1975).
[58] J. H. Chappell and S. S. Murray, Nucl. Instrum. Methods Phys. Res. A **221**, 159 (1984).
[59] I. Holl, E. Lorenz, and G. Mageras, IEEE Trans. Nucl. Sci. **35**, 105 (1988).
[60] J. P. Moy, A. Koch, and M. B. Nielsen, Nucl. Instrum. Methods Phys. Res. A **326**, 581 (1993).
[61] I. A. Kamenskikh, M. A. MacDonald, V. N. Makhov, V. V. Mikhailin, I. H. Munro, and M. A. Terekhin, Nucl. Instrum. Methods Phys. Res. A **348**, 542 (1994).
[62] V. G. Krongauz and I. A. Parfianovich, J. Lumin. **9**, 61 (1974).
[63] A. R. Lubinsky, J. F. Owen, and D. M. Korn, Proc. SPIE **626**, 120 (1986).
[64] D. M. Korn, A. R. Lubinsky, and J. F. Owen, Proc. SPIE **626**, 108 (1986).
[65] A. R. Lubinsky, B. R. Whiting, and J. F. Owen, Proc. SPIE **767**, 167 (1987).
[66] B. R. Whiting, J. F. Owen, and B. H. Rubin, Nucl. Instrum. Methods Phys. Res. A **266**, 628 (1988).
[67] Y. Amemiya, Y. Satow, T. Matsushita, J. Chikawa, K. Wakabayashi, and J. Miyahara, Top. Curr. Chem. **147** (1988).
[68] Y. Amemiya, Synchrotron Radiat. News **3**, 21 (1990).
[69] Robert K. Swank, J. Appl. Phys. **44**, 4199 (1973).
[70] Robert K. Swank, Appl. Opt. **12**, 1865 (1973).
[71] R. K. Swank, J. Appl. Phys. **45**, 3673 (1974).
[72] J. C. Dainty and R. Shaw, *Image Science* (Academic, London, 1974).
[73] J. W. Goodman, *Introduction to Fourier Optics* (McGraw-Hill, New York, 1968).
[74] R. M. Nishikawa and M. J. Yaffe, Med. Phys. **16**, 773 (1989).
[75] P.-C. Wang and G. S. Cargill, J. Appl. Phys. **81**, 1031 (1997).
[76] S. L. Barna, M. W. Tate, S. M. Gruner, and E. F. Eikenberry, Rev. Sci. Instrum. **70**, 2927 (1999).
[77] U. W. Arndt and D. J. Gilmore, Nucl. Instrum. Methods **201**, 13 (1982).
[78] K. Oba, M. Ito, M. Yamaguchi, and M. Tanaka, Adv. Electron. Electron Phys. **74**, 247 (1988).
[79] C. M. Allinson, N. M. Castelli, K. J. Moon, and D. L. Watson, Nucl. Instrum. Methods Phys. Res. A **348**, 649 (1994).
[80] G. T. Reynolds and P. E. Condon, Rev. Sci. Instrum. **28**, 1098 (1957).
[81] P. Ottonello *et al.*, Nucl. Instrum. Methods Phys. Res. A **323**, 485 (1992).
[82] P. Pavan *et al.*, Nucl. Instrum. Methods Phys. Res. A **327**, 600 (1993).
[83] G. Zanella *et al.*, Nucl. Instrum. Methods Phys. Res. A **345**, 198 (1994).
[84] P. Ottonello *et al.*, Nucl. Instrum. Methods Phys. Res. A **346**, 379 (1994).
[85] G. Gennaro *et al.*, Nucl. Instrum. Methods Phys. Res. A **382**, 567 (1996).
[86] S. Costa *et al.*, Nucl. Instrum. Methods Phys. Res. A **380**, 568 (1996).
[87] G. Zanella and R. Zannoni, Nucl. Instrum. Methods Phys. Res. A **406**, 93 (1998).
[88] V. Duchenois, M. Fouassier, and C. Piaget, Adv. Electron. Electron Phys. **64B**, 365 (1985).
[89] G. W. Goetze, Adv. Electron. Electron Phys. **22A**, 219 (1966).
[90] J. E. Bateman and R. J. Apsimon, Adv. Electron. Electron Phys. **52**, 189 (1979).
[91] G. Bertolini and A. Coche, *Semiconductor Detectors* (Wiley Interscience, New York, 1968).
[92] G. Dearnaley and D. C. Northrop, *Semiconductor Counters for Nuclear Radiations* (E. & F. N. Spon, Ltd., London, 1964).
[93] http://www-physics.lbl.gov/~spieler/SLAC_Lectures/index.html.
[94] H. J. Fitting, Phys. Status Solidi A **26**, 525 (1974).
[95] H. Nakatani *et al.*, Nucl. Instrum. Methods Phys. Res. A **283**, 303 (1989).
[96] D. K. Schroder, IEEE Trans. Nucl. Sci. **ED21**, 737 (1974).
[97] C. Frojdh, H. E. Nilsson, P. Nelvig, and C. S. Petersson, IEEE Trans. Nucl. Sci. **45**, 374 (1998).
[98] M. Gambaccini, A. Taibi, P. Baldelli, A. Del Guerra, and A. Tuffanelli, Nucl. Instrum. Methods Phys. Res. A **409**, 508 (1998).
[99] B. P. Flannery, H. E. Deckman, W. G. Roberge, and K. L. D'Amico, Science **237**, 1439 (1987).
[100] H. W. Deckman, K. L. D'Amico, J. H. Dunsmuir, B. P. Flannery, and S. M. Gruner, Adv. X-Ray Anal. **32**, 641 (1989).
[101] H. W. Deckman and S. M. Gruner, Nucl. Instrum. Methods Phys. Res. A **246**, 527 (1986).
[102] W. P. Siegmund, in *Handbook of Optics*, edited by Walter G. and Vaughan Driscoll, William (McGraw-Hill, New York, 1978).
[103] Incom, http://www.incomusa.com/open.html
[104] Schott Fiber Optics, http://www.schottfiberoptics.com/
[105] G. T. Reynolds, J. R. Milch, and S. M. Gruner, Rev. Sci. Instrum. **49**, 1241 (1978).
[106] James B. Hedrick, Am. Ceram. Soc. Bull. **74**, 144 (1995).
[107] We use 3M Scotch Super 33+ tape (St. Paul, MN). Some other brands are insufficiently opaque.
[108] For example, RX22P, Rexon Components, Inc., Macedonia, OH 44056, or GE RTV655, General Electric Co., Waterford, NY 12188.
[109] M. W. Tate, S. M. Gruner, and E. F. Eikenberry, Rev. Sci. Instrum. **68**, 47 (1997).
[110] A. Rose, *Vision. Human and Electronic* (Plenum Press, New York, 1973), Chap. 7.
[111] C. B. Johnson and L. D. Owen, in *Handbook of Optics Vol. 1*, edited by M. Bass (McGraw-Hill, New York, 1995), Vol. 1, pp. 21.1–21.32.
[112] See, for example, http://www.proxitronic.de/prod/bv/eein.htm and http://usa.hamamatsu.com/cmp-pdfs/detectors/Image%20Intensifier_TII%200001E01.pdf.
[113] Y. Amemiya, K. Ito, N. Yagi, Y. Asano, K. Wakabayashi, T. Ueki, and T. Endo, Rev. Sci. Instrum. **66**, 2290 (1995).
[114] J. P. Moy, Nucl. Instrum. Methods Phys. Res. A **348**, 641 (1994).
[115] J. L. Wiza, Nucl. Instrum. Methods **162**, 587 (1979).
[116] B. Rodricks, Q. Huange, R. Hopf, and K. Wang, Nucl. Instrum. Methods Phys. Res. A **348**, 572 (1994).
[117] John L. Lowrance, P. Zucchino, G. Renda, and D. C. Long, Photo-Electronic Image Devices **52**, 441 (1979).
[118] S. M. Gruner, J. R. Milch, and G. T. Reynolds, Rev. Sci. Instrum. **53**, 1770 (1982).
[119] S. M. Gruner, Trans. ACA **34**, 11 (1999).

[120] James A. Hall, in *Applied Optics and Optical Engineering, Vol VIII*, edited by R. R. Shannon and J. C. Wyant (Academic, New York, 1980), Vol. VIII, pp. 349–400.
[121] C. H. Sequin and M. F. Tompsett, *Charge Transfer Devices* (Academic, New York, 1975).
[122] M. J. Morgan and D. V. Howes, *Charge-Coupled Devices and Systems* (Wiley, New York, 1979).
[123] T. J. Tredwell, in *Handbook of Optics, Vol I*, edited by M. Bass (McGraw-Hill, New York, 1995), Chap. 22, pp. 22.1–22.38.
[124] G. C. Holst, in *Handbook of Optics, Vol III*, edited by M. Bass (McGraw-Hill, New York, 2001), pp. 4.1–4.22.
[125] Listings are available through the SPIE web site at www.spie.org
[126] C. Buil, *CCD Astronomy: Construction and Use of an Astronomical CCD Camera* (Willmann-Bell, Richmond, VA, 1991).
[127] R. Berry, V. Kanto, and J. Munger, *The CCD Camera Cookbook: How to Build Your Own CCD Camera* (Willmann-Bell, Richmond, VA, 1994).
[128] D. Walton, R. A. Stern, R. C. Catura, and J. L. Culhane, Proc. SPIE **501**, 306 (1984).
[129] L. Struder, G. Lutz, M. Sterzik, P. Holl, J. Kemmer, U. Prechtel, and T. Ziemann, IEEE Trans. Nucl. Sci. **35**, 372 (1988).
[130] L. Struder, H. Brauninger, G. Lutz, M. Meier, P. Predehl, M. Sterzik, J. Kemmer, and P. Rehak, Proc. SPIE **982**, 129 (1988).
[131] H. Brauninger, G. Lutz, N. Meidinger, P. Predehl, C. Reppin, W. Schreiber, L. Struder, J. Trumper, E. Kenziora, G. Staubert, V. Radeka, P. Rehak, S. Rescia, E. Gatti, A. Longoni, M. Sampietro, P. Holl, J. Kemmer, U. Prechtel, H. Riedel, and T. Ziemann, Proc. SPIE **1344**, 404 (1990).
[132] D. J. Burt, presented at the ESA Symposium on Photon Detectors for Space Instrumentation, 10–12 November 1992 (ESA/ESTEC, Noordwijk, The Netherlands, 1993).
[133] R. J. Stover, M. Wei, Y. Lee, D. K. Gilmore, S. E. Holland, D. E. Groom, W. W. Moses, S. Perlmutter, G. Goldhaber, C. Pennypacker, N. W. Wang, and N. Palaio, Proc. SPIE **3019**, 183 (1997).
[134] D. H. Lumb, G. R. Hopkinson, and A. A. Wells, Adv. Electron. Electron Phys. **64B**, 498 (1985).
[135] David H. Lumb and Andrew D. Holland, Proc. SPIE **982**, 116 (1988).
[136] N. M. Allinson, R. Brammer, J. R. Helliwell, S. Harrop, B. G. Magorrian, and T. Wan, J. Sol-Gel Sci. Technol. **1**, 143 (1989).
[137] N. M. Allinson, M. Colapietro, J. R. Helliwell, K. J. Moon, A. W. Thompson, and S. Weisberger, Rev. Sci. Instrum. **63**, 664 (1992).
[138] D. H. Lumb and J. A. Nousek, IEEE Trans. Nucl. Sci. **39**, 1379 (1992).
[139] K. J. Moon, N. M. Allinson, and J. R. Helliwell, Nucl. Instrum. Methods Phys. Res. A **348**, 631 (1994).
[140] F. A. Sachs and P. E. Howard, Electro-Opt. Syst. Des. **7**, 34 (1975).
[141] R. S. Aikens, C. R. Lynds, and R. E. Nelson, Proc. SPIE **78**, 65 (1976).
[142] H. K. Burke and G. J. Michon, IEEE J. Solid-State Circuits **11**, 121 (1976).
[143] D. M. Brown, M. Ghezzo, and M. Garfinkel, IEEE J. Solid-State Circuits **11**, 128 (1976).
[144] Q. S. Hanley, J. B. True, and M. B. Denton, J. Synchrotron Radiat. **2**, 215 (1995).
[145] E. R. Fossum, Nucl. Instrum. Methods Phys. Res. A **395**, 291 (1997).
[146] P. Gwynne, IEEE Spectrum **38**, 27 (2001).
[147] D. Litwiller, Photonics Spectra **35**, 154 (2001).
[148] C. Ponchut, Nucl. Instrum. Methods Phys. Res. A **457**, 270 (2001).
[149] H. S. Wong, IEEE Trans. Electron Devices **43**, 2131 (1996).
[150] E. F. Eikenberry, S. M. Gruner, and J. L. Lowrance, IEEE Trans. Nucl. Sci. **33**, 542 (1986).
[151] H. Roehrig, T. W. Ovitt, W. J. Dallas, R. D. Lamoreaux, R. Vercillo, and K. M. McNeill, Proc. SPIE **767**, 144 (1987).
[152] M. G. Strauss, I. Naday, I. S. Sherman, M. R. Kraimer, and E. M. Westbrook, IEEE Trans. Nucl. Sci. **NS-34**, 389 (1987).
[153] I. Naday, M. G. Strauss, I. S. Sherman, M. R. Kraimer, and E. M. Westbrook, Opt. Eng. **26**, 788 (1987).
[154] M. G. Strauss, I. Naday, I. S. Sherman, M. R. Kraimer, E. K. Westbrook, and N. J. Zaluzec, Nucl. Instrum. Methods Phys. Res. A **266**, 563 (1988).
[155] J. Widom, Rev. Sci. Instrum. **60**, 3231 (1989).
[156] M. G. Strauss, E. M. Westbrook, I. Naday, T. A. Coleman, M. L. Westbrook, D. J. Travis, R. M. Sweet, J. W. Pflugrath, and M. Stanton, Nucl. Instrum. Methods Phys. Res. A **297**, 275 (1990).
[157] K. Kalata, W. C. Phillips, M. Stanton, and Y. Li, Proc. SPIE **1345**, 270 (1990).
[158] K. Nakajima, S. Sudo, and S. Aoki, Jpn. J. Appl. Phys., Part 1 **32**, 5754 (1993).
[159] B. Chu, P. J. Harney, Y. Li, K. Linliu, and F. Yeh, Rev. Sci. Instrum. **65**, 597 (1994).
[160] J. H. Kinney, Q. C. Johnson, U. Bonse, R. Nusshardt, and M. C. Nicols, Proc. SPIE **691**, 43 (1986).
[161] R. Germer and W. Meyer-Ilse, Rev. Sci. Instrum. **57**, 426 (1986).
[162] B. Rodricks, R. Clarke, R. Smither, and A. Fontaine, Rev. Sci. Instrum. **60**, 2586 (1989).
[163] H. F. Fuchs, D. Q. Wu, and B. Chu, Rev. Sci. Instrum. **61**, 712 (1990).
[164] E. F. Eikenberry, M. W. Tate, A. L. Belmonte, J. L. Lowrance, D. Bilderback, and S. M. Gruner, IEEE Trans. Nucl. Sci. **38**, 110 (1991).
[165] B. Chu, J. Rousseau, and T. Gao, Rev. Sci. Instrum. **63**, 4000 (1992).
[166] A. Koch, Nucl. Instrum. Methods Phys. Res. A **348**, 275 (1994).
[167] I. Naday, S. Ross, M. Kanyo, M. L. Westbrook, and E. M. Westbrook, Proc. SPIE **2415**, 236 (1995).
[168] E. Pace and G. Naletto, Proc. SPIE **2519**, 149 (1995).
[169] R. Pahl, Proc. SPIE **2519**, 135 (1995).
[170] A. R. Faruqi, H. N. Andrews, and R. Henderson, Nucl. Instrum. Methods Phys. Res. A **367**, 408 (1995).
[171] A. Koch and C. Riekel, Rev. Sci. Instrum. **67**, 1737 (1996).
[172] I. Ross, S. Westbrook, E. M. Zentai, and G. Naday, Opt. Eng. **37**, 1235 (1998).
[173] A. R. Faruqi, in *Mechanisms of Work Production and Work Absorption in Muscle* (Plenum, New York, 1998), pp. 63–72.
[174] A. R. Faruqi, R. Henderson, and S. Subramaniam, Ultramicroscopy **75**, 235 (1999).
[175] N. M. Allinson, Nucl. Instrum. Methods Phys. Res. A **275**, 587 (1989).
[176] R. Clarke and B. Rodricks, Rev. Sci. Instrum. **60**, 2280 (1989).
[177] H. Tsunemi, S. Kawai, and K. Hayashida, Jpn. J. Appl. Phys., Part 1 **30**, 1299 (1991).
[178] H. N. Chapman, C. Jacobsen, and S. Williams, Rev. Sci. Instrum. **66**, 1332 (1995).
[179] L. Struder, C. Fiorini, E. Gatti, R. Hartmann, P. Holl, N. Krause, P. Lechner, A. Longoni, G. Lutz, J. Kemmer, N. Meidinger, M. Popp, H. Soltau, U. Weber, and C. von Zanthier, J. Synchrotron Radiat. **5**, 268 (1998).
[180] N. M. Allinson, Nucl. Instrum. Methods **201**, 53 (1982).
[181] R. Clarke, Nucl. Instrum. Methods Phys. Res. A **291**, 117 (1990).
[182] R. Clarke, Nucl. Instrum. Methods Phys. Res. A **347**, 529 (1994).
[183] E. M. Westbrook and I. Naday, Methods Enzymol. **276**, 244 (1997).
[184] S. M. Gruner, J. R. Milch, and G. T. Reynolds, IEEE Trans. Nucl. Sci. **NS-25**, 562 (1978).
[185] D. J. Thomas, Proc. R. Soc. London, Ser. A **425**, 129 (1989).
[186] M. Stanton, W. C. Phillips, Y. Li, and K. Kalata, J. Appl. Crystallogr. **25**, 549 (1992).
[187] W. C. Phillips, Y. Li, M. Stanton, J. Xie, D. O'Mara, and K. Kalata, Nucl. Instrum. Methods Phys. Res. A **334**, 621 (1993).
[188] A. P. Hammersley, S. O. Svensson, and A. Thompson, Nucl. Instrum. Methods Phys. Res. A **346**, 312 (1994).
[189] A. P. Hammersley, S. O. Svensson, A. Thompson, H. Graafsma, A. Kvick, and J. P. Moy, Rev. Sci. Instrum. **66**, 1 (1995).
[190] J. P. Moy, A. P. Hammersley, S. O. Svensson, A. Thompson, K. Brown, L. Claustre, A. Gonzalez, and S. McSweeney, J. Synchrotron Radiat. **3**, 1 (1996).
[191] A. P. Hammersley, K. Brown, W. Burmeister, L. Claustre, A. Gonzalez, S. McSweeney, E. Mitchell, J.-P. Moy, S. O. Svensson, and A. W. Thompson, J. Synchrotron Radiat. **4**, 67 (1997).
[192] E. Breitanberger, Prog. Nucl. Phys. **4**, 56 (1955).
[193] U. W. Arndt and D. J. Gilmore, J. Appl. Crystallogr. **12**, 1 (1979).
[194] S. M. Gruner and J. R. Milch, Transactions ACA **18**, 149 (1982).
[195] M. Stanton, W. Phillips, Y. Li, and K. Kalata, J. Appl. Crystallogr. **25**, 638 (1992).
[196] M. Stanton, W. Phillips, Y. Li, and K. Kalata, Nucl. Instrum. Methods Phys. Res. A **325**, 550 (1992).
[197] M. W. Tate, E. F. Eikenberry, S. L. Barna, M. E. Wall, J. L. Lowrance, and S. M. Gruner, J. Appl. Crystallogr. **28**, 196 (1995).
[198] S. L. Shapiro, W. M. Dunwoode, J. F. Arens, J. G. Jernigan, and S. Gaalema, Nucl. Instrum. Methods Phys. Res. A **275**, 580 (1989).
[199] E. H. M. Heijne, Phys. Medica **9**, 109 (1993).
[200] P. Delpierre, J. Phys. IV **4**, C9-11-18 (1994).
[201] F. Arfelli, G. Barbiellini, G. Cantatore, E. Castelli, P. Cristaudo, L. Dalla Palma, M. Di Michiel, R. Longo, P. Poropat, R. Rosei, M. Sessa, F. Tomasini, G. Tromba, and A. Vacchi, Nucl. Instrum. Methods Phys. Res. A **353**, 366 (1994).
[202] P. Hausmann, J. Overdick, M. Raith, B. Wermes, N. Blanquart, L. Bon-

zom, V. Delpierre, and P. Fischer, Nucl. Instrum. Methods Phys. Res. A **405**, 53 (1997).
[203] P. Datte, A. Birkbeck, E. Beuville, N. Endres, F. Druillole, L. Luo, J. Millaud, and N.-H. Xuong, Nucl. Instrum. Methods Phys. Res. A **421**, 576 (1999).
[204] G. Rossi, M. Renzi, E. F. Eikenberry, M. W. Tate, D. Bilderback, E. Fontes, R. Wixted, S. Barna, and S. M. Gruner, J. Synchrotron Radiat. **6**, 1096 (1999).
[205] P. J. Sellin, G. Rossi, M. J. Renzi, A. P. Knights, E. F. Eikenberry, M. W. Tate, S. L. Barna, R. L. Wixted, and S. M. Gruner, Nucl. Instrum. Methods Phys. Res. A **460**, 207 (2001).
[206] Ch. Broennimann, R. Baur, E. F. Eikenberry, S. Kohout, M. Lindner, B. Scmitt, and R. Horisberger, Nucl. Instrum. Methods Phys. Res. A **465**, 235 (2001).
[207] D. J. Burt, Nucl. Instrum. Methods Phys. Res. A **305**, 564 (1991).
[208] The CCD Image Sensor, Thomson-CSF, Orsay, France.